The following manuscript was unavailable at the time of publication.

DEVELOPMENT WORK IN SUPPORT OF B&W'S LOW EMISSION BOILER SYSTEM

G.A. Farthing
Babcock & Wilcox Company
2o South Van Buren Avenue
Barberton, OH 44203

Please contact author(s) for a copy of this paper.

ADVANCED RESEARCH & TECHNOLOGY DEVELOPMENT SESSION

KINETICS AND MECHANISMS OF COAL CHAR COMBUSTION AND CARBON BURNOUT

CONTRACT NUMBER: FWP 0709

CONTRACTOR: Combustion Research Facility
Sandia National Laboratories
Livermore, CA 94551-0969

PRINCIPAL INVESTIGATORS:

Robert H. Hurt;	(510) 294-3707
Kevin A. Davis	(510) 294-2474
Nancy Y. C. Yang	(510) 294-2680
Donald R. Hardesty	(510) 294-2321

DOE PROJECT MANAGEMENT: Philip Goldberg, James Hickerson

BACKGROUND AND PROJECT OBJECTIVE

The amount of unburned carbon in fly ash is an important concern in the design and operation of pulverized coal fired boilers, affecting combustion efficiency, boiler performance, and ash marketability. The late stages of char combustion have a special technological significance, as carbon conversions of 99% or greater are typically required for the economic operation of commercial-scale systems. Achieving such high conversions is difficult in certain cases, especially in connection with boilers retrofitted with combustion zone modifications for NO_x abatement [Fiveland and Jamaluddin, 1992]. While there is an extensive literature on ignition [Essenhigh et al., 1989], and char combustion [Field, 1970, Smith, 1982, Essenhigh, 1981], there have been many fewer studies of extinction [Mulcahy, 1977], conversion-dependent reactivities [Hecker et al., 1992, Charpenay et al., 1992], or the important late stages of combustion, in part due to the difficulty of making scientifically meaningful measurements on highly reacted samples in which inorganic material (ash) is the majority constituent.

In Sandia's Coal Combustion Laboratory (CCL), unique optical techniques and advanced materials analytical facilitates are developed and used to determine char oxidation kinetics with an emphasis on the late stages of combustion. Experiments are performed on a suite of commercially-important U.S. coals of various rank and type, as well as residual carbon materials extracted from fly ash samples from commercial-scale coal combustors. The ultimate goal of the project is the development of an advanced, time-dependent kinetic model that predicts the combustion rates and burnout times of chars over a wide range of conditions of interest to current and future pulverized coal combustion technologies.

SUMMARY OF ACCOMPLISHMENTS

In FY93-94, a new experimental apparatus for captive particle imaging was developed in the CCL and used for the investigation of char combustion behavior in the critical high-conversion regime. These results, coupled to *in-situ* optical measurements in the entrained flow reactor generated important new insights into reactivity loss, extinction-phenomena, and the late stages of burnout. Char reactivity was observed to decrease substantially during combustion, and advanced materials analytical facilities at Sandia were applied to partially-reacted chars to understand the mechanisms for reactivity loss. The analytical techniques include laser spark spectroscopy, X-ray diffraction, solid-phase FTIR, and high resolution transmission electron microscopy fringe imaging with digital image analysis. The development of the captive particle

imaging apparatus is described in the following section and subsequent sections present and discuss a selection of recent research results.

Development of the Captive Particle Imaging Apparatus

Figure 1 depicts the new captive particle imaging (CPI) apparatus, developed in FY93-94. Coal or char particles of 50 - 300 μm in diameter are placed on a low-density particle support and inserted into the flow reactor through a open test section in the quartz wall. The support is surrounded by a small conical cooling coil which maintains the particle at 200 - 300 °C, while it is brought into the focal volume of a modified long-focal-length microscope. The cooling coil is then retracted, the particle is rapidly heated by the surrounding gases, and its ignition, combustion, and burnout behavior is imaged at high resolution using both reflected visible light and emitted radiation in the near infrared.

The particle support consists of a platinum ring, spanned in several places by 75 μm diameter platinum wires that provide support for a thin layer of fine (5 μm diameter) Al_2O_3 fibers, having an ultra-low solid volume fraction. Because transport processes for particles in the pulverized size range are dominated by diffusion, conduction, and radiation, and not by convection [Field, 1970], this mechanical suspension technique accurately simulates char combustion in entrained flows, although it visibly perturbs the flow field and the convective processes. The flow field and the temperature transients at the beginning of the experiment have been characterized by photographic imaging of seeded flows and by fine-wire thermocouples. Maximum heating rates are approximately $2 \cdot 10^3$ K/sec with good shot-to-shot reproducibility. The rapid and reproducible temperature transients combined with the avoidance of transients in gas composition make this flow configuration useful for investigating char combustion and burnout phenomena. The optical system comprises a long-focal-length microscope modified by addition of an internal beam splitter to allow simultaneous dual video imaging of the same field-of-view. A CCD camera records an image formed by reflected visible light (supplied by fiber-optic illumination) while a second camera registers an image formed by near-infrared emission from

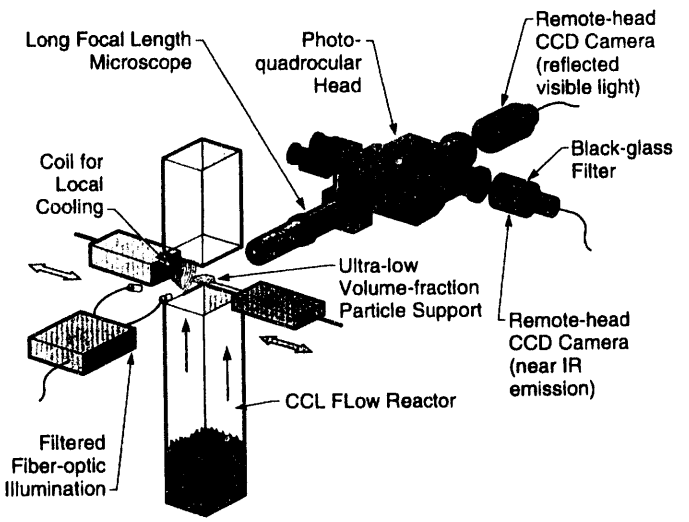

Figure 1. Schematic of the captive particle imaging apparatus. Analog and digital image acquisition, storage, and processing hardware is not shown.

the particle surfaces. The near-infrared channel has been calibrated with a high-temperature black-body source and the thermographic images are digitized and quantitatively analyzed to determine particle radiance temperatures.

The Late Stages of Char Combustion

The late stages of char combustion were investigated in FY94 by two independent optical techniques. The first technique uses *in situ* optical measurements on entrained char particles burning in a laminar flow reactor, coupled with a criterion developed at Sandia [Hurt, 1993] for distinguishing inorganic from carbon-rich particles by measurement of their spectral emissive factors in the near-infrared. The second technique employs the new captive-particle imaging apparatus equipped for simultaneous near-infrared thermography.

Captive particle image sequences were obtained for approximately one-hundred particles of Illinois #6, Pittsburgh #8, and Pocahontas #3 coal chars. An example dual image sequence is shown in Fig. 3, along with time-resolved radiance temperatures determined from digitization of the near-infrared images. The combined data and images show a period of bright incandescence from 0.8 to 1.2 seconds, followed by a relatively abrupt drop in temperature of 125 K and a long, slow, nearly-isothermal, final burnout to a carbon-free ash particle. This event has been referred

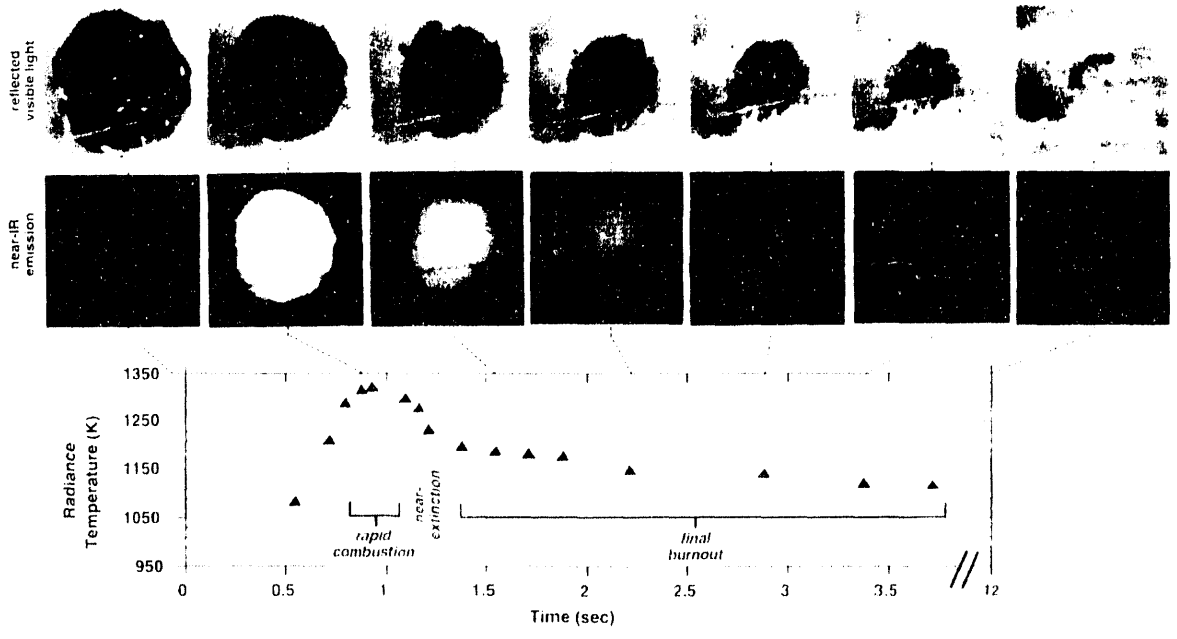

Figure 2. Dual-camera captive particle image sequence for typical Illinois #6 coal char particle. Combustion of ≈200 μm particle in 6 mole-% oxygen at a steady-state local gas temperature of 1250 K.

to as a near-extinction [Hurt, 1993], and it significantly increases the time required for complete combustion. The dual image sequences are particularly useful for defining the point of near-extinction—it occurs while the particle is still dark under visible illumination, often before the appearance of any visible surface ash. Near-extinction is also observed for particles containing very small amounts of mineral matter (as inferred from the size of the final ash particle). For these low-ash particles, the near-extinction is clearly not caused by the formation of an ash-film diffusion barrier.

For particles with a high mineral content initially, the final stage of the combustion process consists of the removal of these elemental carbon inclusions from a predominately inorganic matrix. This process, which we refer to here as "ash decarburization" can be extremely slow, requiring from 1-2 orders of magnitude more time than the duration of the primary, rapid combustion stage. Another unique characteristic of high-mineral-content particles is that their combustion and burnout generally occurs without dramatic changes in the particle morphology or size. The mineral matter provides a cohesive framework from which elemental carbon is removed while preserving much of the original particle shape. No fragmentation, or structural rearrangement of the particles is typically observed. The ash frameworks, however, are often observed to slowly consolidate and densify after most of the carbon disappears, due perhaps to sintering mechanisms.

Low-mineral-content, low-density particles, in contrast, undergo profound morphological changes during combustion. Consumption of carbon from these particles often results in loosely connected, fragile structures at moderate to high conversion. Such particles are much more likely to fragment during combustion, but instead of producing distinct fragments as has been observed for entrained particles [Baxter, 1992], they are typically observed to contract or reagglomerate to yield a single ash particle.

In addition to the captive particle results, *in situ* optical measurement of single-particle size, temperature, and emissive factor have been made during combustion to high carbon conversion in an entrained-flow reactor. These data indicate a gradual transition from a population of fully ignited char particles in the early-stages of char combustion to a predominance of low-temperature particles at a char carbon conversion of 75% and, finally, to a predominance of inorganic-rich particles (with emissive factors < 0.3) at a char carbon conversion of >90%. After eliminating inorganic particles from the analysis [Hurt, 1993], conversion-dependent kinetics were computed from the optical data and are plotted in Fig. 3. The reactivity in Fig. 3 decreases monotonically during combustion, dropping by a factor of 5 at 90% conversion. This reactivity loss occurs in a region where the degree of carbon crystallinity in the sample is increasing sharply, as discussed in the next section.

The Evolution of Carbon Crystalline Structure During Combustion

To help explain the observed loss of global char reactivity during combustion, the evolution of the organic char matrix was characterized for selected samples in FY94. The characterization included measurements of elemental hydrogen, elemental oxygen, total surface area by carbon dioxide vapor adsorption, as well as application of X-ray diffraction (XRD), and high resolution transmission electron microscopy (HRTEM) fringe imaging. Although HRTEM fringe imaging has been widely applied to other carbon materials, the current effort represents the first attempts, to the authors' knowledge, to apply it to the study of coal char transformations during combustion. The HRTEM technique is illustrated in Fig. 4. A char sample is hand-ground to a fine powder, placed on a holey carbon grid, and then examined at moderate magnification to find wedge-shaped fragments that are optically thin at the edge (see left hand image in Fig 4). A number of such edge regions (typically ten or more) are then photographed at high

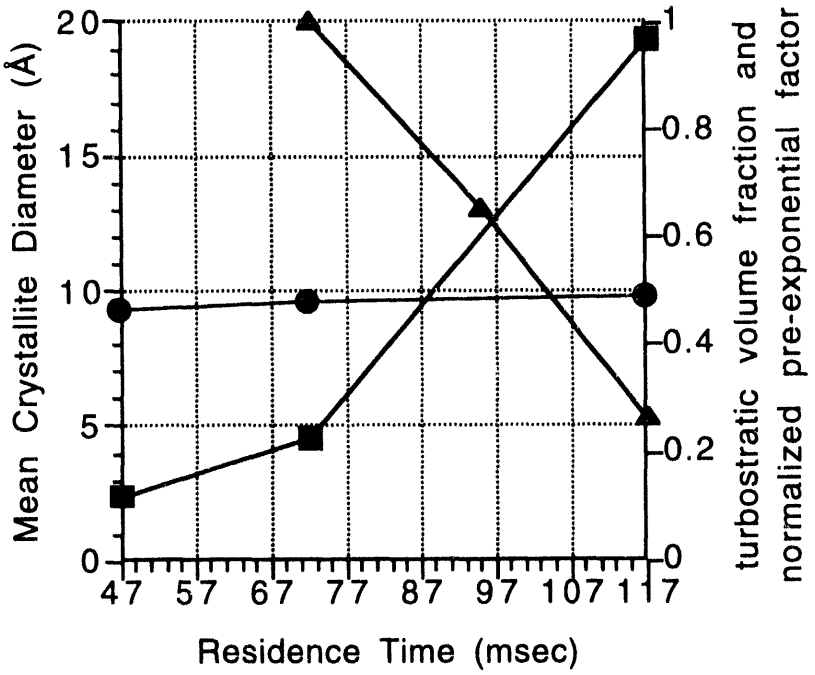

Fig. 3. Mean crystallite diameter (circles), turbostratic volume fraction (squares), and char reactivity or preexponential factor (triangles) as a function of residence time for partially-combusted Illinois #6 coal chars samples from the Sandia entrained flow reactor. Crystallite size parameters were determined by digital analysis of HRTEM fringe images.

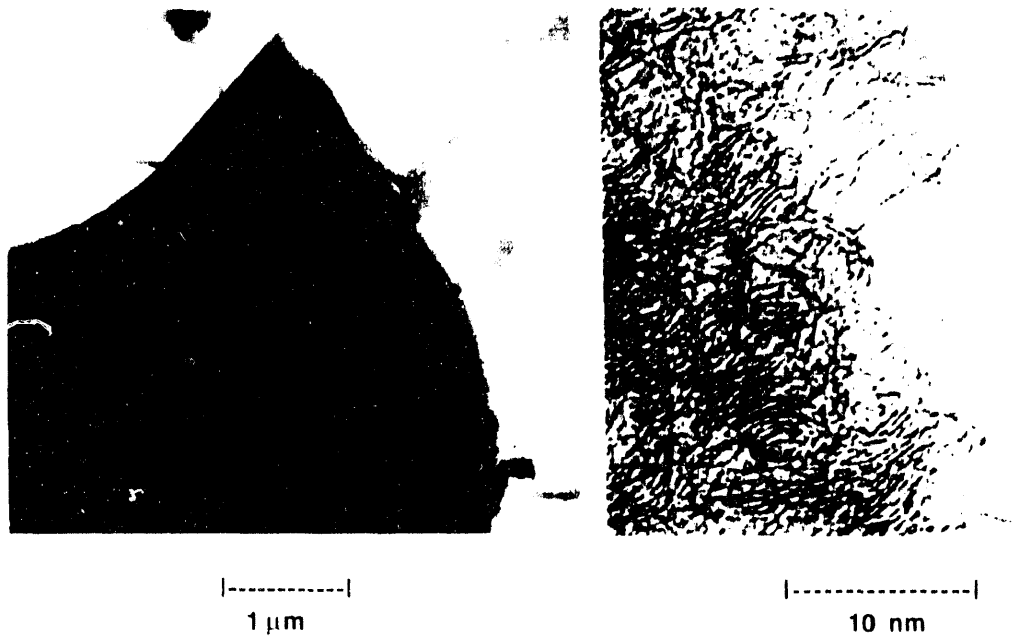

Figure 4. Illustration of technique used to obtain high resolution transmission electron microscopy (HRTEM) fringe images of coal char and residual carbon samples. Left panel is low magnification image of a residual carbon fragment (the large dark body) residing on a holey carbon grid. Right panel is a high magnification fringe image of the optically thin regions near the edge of the same carbon fragment.

magnifications (approximately 2,000,000 x) in fringe imaging mode, and representative fields of view selected and reproduced (see right hand image in Fig 4). Individual graphitic layers with their planes perpendicular to the image plane are clearly distinguishable in Fig. 4 as lines, separated by a distance that approximates, but is typically somewhat greater than, the characteristic interlayer spacing for crystalline graphite, 0.335 nm. HRTEM fringe images yield a wealth of information on the degree and nature of crystallinity in carbons, including interlayer spacings, the dimensions (lengths) of the graphitic layers and the extent of parallel alignment of neighboring layers (stacking depths).

Fringe images were obtained for a series of partially reacted Illinois #6 char samples and several residual carbon samples from commercial-scale boilers. The young char sampled at the end of the primary devolatilization zone was observed to be highly amorphous, with individual, curved carbon fringes predominating. At 72 msec, corresponding to 24% char carbon conversion, most of the fringe image fields examined were still amorphous, with a minority showing some recognizable turbostratic crystallinity. The carbon crystalline structure continues to develop from 72 to 117 msec, with the sample at 117 msec (76% conversion) exhibiting stacking depths of up to 10 layers and fringe lengths of up to 10 nm. The development of crystalline order under combustion conditions has also been noted by Levendis and Flagan [1989] for polymer-derived carbons, and to a lesser extent for biomass-derived chars [Wornat et al., 1994]. The lack of crystalline order developed in biomass chars produced under conditions similar to those in the present work can be attributed to the high oxygen-content and structural rigidity in the nonfusible parent material [Wornat et al., 1994].

A custom digital image analysis algorithm was developed to measure fringe or crystallite size statistics and thus to quantify the increase in crystalline order observed by HRTEM. The results are summarized in Fig. 3. Mean diameters are shown to increase only slightly with residence time, which is qualitatively similar to the XRD results. An alternative metric for degree of crystallinity that can be derived from the images is the total volume of material in a recognizable

turbostratic structure. This parameter increases slightly from 47 to 72 msec before undergoing a rapid increase from 72 to 117 msec at the same time that the global reactivity (preexponential factor) is decreasing. Among the four indicators of the organic char structure evaluated (H/C ratio, carbon dioxide surface area, crystallite dimensions by X-ray diffraction, and HRTEM images), the volume fraction of turbostratically ordered material as determined by HRTEM fringe-imaging correlates best with the observed reactivity loss for Illinois #6 coal chars and residual carbon samples.

DISCUSSION AND CONCLUSIONS

The combination of *in situ* optical measurements and independent captive particle image sequences provide dramatic illustration of the asymptotic nature of the char burnout process. Single particle combustion to complete burnout comprises two distinct stages: (1) a rapid high-temperature combustion stage, consuming approximately 70% of the char carbon and ending with near-extinction of the heterogeneous reactions due to loss of global particle reactivity, and (2) a final burnout stage occurring slowly and at lower temperatures. For particles containing significant amounts of mineral matter, the second stage can be further subdivided into: (2a) late char combustion, which begins after a near-extinction event, and converts carbon-rich particles to mixed particle types at a lower temperature and a slower rate; and (2b) decarburization of ash — the removal of residual carbon inclusions from inorganic (ash) frameworks in the very late stages of combustion. This latter process can be extremely slow, requiring over an order of magnitude more time than the primary rapid combustion stage.

The low global reactivities of inorganic-rich particles is not surprising, as mineral matter can act as a diffusion barrier, or simply as a "diluent" [Hurt et al., 1994], reducing the carbon surface area per unit *particle* volume. A more significant observation is the initial temperature drop, that we refer to as a near-extinction event, which is exhibited by most of the particles investigated. The near-extinction is caused by a loss of global reactivity, and occurs for both high and very low ash content particles, often before ash becomes visible on the particle surfaces. For particles with very little ash, the loss of global reactivity is likely related to changes in the carbonaceous phase, rather than interactions with the bulk mineral matter.

Separate experiments were therefore performed to characterize the evolution of the organic char matrix during high temperature combustion. When pulverized-coal particles are rapidly heated by injection into a hot oxidizing environment, the processes of devolatilization, carbon structural ordering, and heterogeneous oxidation occur sequentially, but with significant overlap. Unlike experiments in which the char is stabilized by heat treatment prior to combustion, entrained flow reactor experiments (and most practical devices) yield a young char that is highly amorphous, highly reactive, and possesses high surface area and residual hydrogen content during the early stages of combustion. The early stages of heterogeneous oxidation proceed in parallel with the latter stages of carbonization, leading to preferential loss of hydrogen, a reduction in surface area, and the development of crystalline order. For highly oxygenated, cross-linked chars derived from biomass, the extent of ordering during combustion is not as great [Wornat, et al., 1994].

Crystalline order is induced in carbon lattices by thermally-driven atomic or mesoscale rearrangements [Marsh et al., 1991, Suuberg, 1991], possibly enhanced by oxidative removal of carbon atoms from the lattice [Hurt et al., 1993, Levendis and Flagan, 1989]. The degree of crystalline order is therefore believed to be primarily determined by the temperature history of the samples, although it may be enhanced by the oxidation or by the preferential consumption of less ordered material. Typical combustion times and peak temperatures are insufficient to bring about true (three dimensional) graphitization for most coals, but rather lead to the growth of regions with turbostratic order, a process we refer to as pregraphitization. The development of turbostratic order is seen to occur gradually over a time scale comparable to the combustion process itself — here, on the order of 100 msec at particle temperatures of 1800 K and oxygen concentrations of 12 mole-%.

Implications: pregraphitization and char deactivation in boilers

The pregraphitization phenomenon has important implications for combustion systems. First, it is intrinsically more difficult to achieve high carbon burnout than is predicted by models based on laboratory char oxidation kinetics. Existing global models used in comprehensive combustion codes do not predict the asymptotic nature of char combustion to complete conversion. Secondly, to identify problem coals with respect to carbon burnout, one must consider both their early combustion reactivity (as is commonly measured in the laboratory) and the propensity of the char to pregraphitize and deactivate at high temperature. Thirdly, char reactivity may be greatly affected by changes in the structure of the flame zone in a boiler. High flame temperatures, for example, may accelerate combustion only slightly (as the heterogeneous reactions are limited at high temperature by the low energy process of boundary-layer diffusion), but may promote char pregraphitization and deactivation, making subsequent complete burnout in the upper furnace region more difficult to achieve. Pregraphitization may be especially detrimental in low NOx systems, where oxidation is delayed and the opportunity may be lost to rapidly consume the young, reactive char. More realistic time-, conversion-, and environment-dependent kinetic models are under development, which will be capable of quantifying these effects and making accurate predictions in the conversion and temperature ranges of industrial interest.

ACKNOWLEDGMENTS

Financial support for this work is provided by the U.S. DOE Pittsburgh Energy Technology Center's Direct Utilization Advanced Research and Technology Development Program. The technical contributions of James Ross, Ja Lee Yio, Douglas Medlin, Richard Yee, C. Scott Kelley, Carlos Gethers, F. William Kent, and Arun Mehta are gratefully acknowledged.

REFERENCES

Baxter, L. L. *Combustion and Flame* 90, 174-184 (1992).

Charpenay, S., Serio, M.A., and Solomon, P.R. *24th Symposium (International) on Combustion*, The Combustion Institute, Pittsburgh, 1992, p. 1189.

Essenhigh, R. H., in *Chemistry of Coal Utilization, Second Supplementary Volume* (M.A. Elliot, Ed.) John Wiley and Sons, New York, 1981, p. 1153.

Essenhigh, R. H., Misra, M. K., and Shaw, D. W., *Comb. and Flame* 77, 3-30 (1989).

Field, M. A., *Combustion and Flame* 14, 237-252 (1970).

Fiveland, W. A., and Jamaluddin, A. S., *Combust. Sci. and Tech.*, 81, 147-167 (1992).

Hecker, W. C., McDonald, K. M., Reade, W., Swensen, M. R., and Cope, R. F. *Twenty-Fourth (International) Symposium on Combustion*, The Combustion Institute, Pittsburgh, 1992, pp. 1225-1231.

Hurt, R. H. *Energy and Fuels* 7, 721-733 (1993)

Hurt, R. H. and R. E. Mitchell. "Unified High-Temperature Char Combustion Kinetics for a Suite of Coals of Various Rank" *24th International Symposium on Combustion*, The Combustion Institute, Pittsburgh, PA, 1992 pp. 1243 - 1250.

Hurt, R. H., Sarofim, A. F., and Longwell, J. P. *Combustion and Flame*, 95, 430 (1993).

Hurt, R. H. and Davis, K. A., "Near-Extinction and Final Burnout in Coal Combustion," accepted for publication in the *Proceedings of the Twenty-Fifth (International) Symposium on Combustion*, 1994

Davis, K. A., Hurt, R. H., Yang, N. Y. C., and Headley, T. H., "Evolution of Char Chemistry, Crystallinity, and Ultrafine Structure during Pulverized Coal Combustion," accepted for publication in *Combustion and Flame*, 1994.

Wornat, M. J., R. H. Hurt,, N . Y. C. Yang, and T. H. Headley, "Structural and Compositional Transformations in Biomass Chars during Combustion" accepted for publication in *Combustion and Flame*, 1994.

Levendis, Y.A. and Flagan, R.C. *Carbon*, 27:265 (1989).

Marsh, H., Diez, M.A., and Kuo, K., in *Fundamental Issues in Control of Carbon Gasification Reactivity* (J. Lahaye and P. Ehrburger, Ed.), 1991, Kluwer Academic Publishers, the Netherlands, p. 205-220.

Mulcahy, M.F.R. "The Combustion of Carbon," in Oxygen in the Metal and Gaseous Fuel Industries, The Chemical Society, London, 1977, p. 175.

Radovic, L.R., Walker. P.L., and R.G., J. *Fuel* 62, 849 (1983).

Smith I. W., *Nineteenth Symposium (International) on Combustion*, The Combustion Institute, Pittsburgh, 1982, pp. 1045-1065.

Smith, I. W., and Tyler, R. J., *Fuel* 51, 312-321 (1972).

Suuberg, E. M. in *Fundamental Issues in Control of Carbon Gasification Reactivity*, Kluwer Academic Publishers, 1991, pp. 269-305.

The following manuscript was unavailable at the time of publication.

THERMODYNAMIC PROPERTIES OF PULVERIZED COAL DURING RAPID HEATING DEVOLATILIZATION PROCESS

W. Proscia
United Technologies Research Center
Silver Lane
East Hartford, CT 06108

Please contact author(s) for a copy of this paper.

10 th Annual DOE-PETC Coal PUEC Contractor's Meeting, July 18-21, 1994

RESEARCH ON FUNDAMENTAL ASPECTS OF INORGANIC PARTICLE DEPOSITION IN COAL-FIRED EQUIPMENT

Daniel E. Rosner

Yale University, Department of Chemical Engineering
High Temperature Chemical Reaction Engineering Laboratory
New Haven, CT 06520-2159 USA

Grant DE FG-22-90PC90099 9/6/90-8/31/94

ABSTRACT

We review here results of our recent research on the *deposition dynamics of combustion-generated particles* in coal-fired power production technologies. In this summary* we outline and illustrate the results of our recently developed methods to predict total surface *deposition rates and associated convective heat transfer reductions* for cylindrical targets exposed to distribution of particles suspended in the mainstream. By combining the essential features of recently developed *single particle sticking probability laws* with our correlation of the *inertial impaction* of particles on a circular cylinder in high Reynolds number cross-flow, we develop formulae and 'universal' graphs which provide the dependence of particle deposition rates, and associated reductions in convective heat transfer, on such system parameters as mainstream velocity, mean particle size and target diameter. The deposition rate prediction procedures illustrated here (see Rosner and Tandon, 1994) are efficient enough to be incorporated into future, improved 'fouling propensity indices' and can also be used to motivate, evaluate and implement "ruggedization" and/or *fouling reduction strategies*.

Details on these theoretical studies (Section 2), and their immediate antecedents, will be found in our archival references (Section 4). A judicious blend of (numerical and physical) experiments, theory, and intuition will continue to be necessary to economically arrive at methods/results to improve the generality and accuracy of future particle-deposition-related design calculations for a wide variety of equipment/fuel types. We propose that our computational and correlation methods be extended to treat more complex situations of practical importance in power generation applications.

1. BACKGROUND and OBJECTIVES

Initially clean heat exchanger surfaces exposed to high temperature flowing suspensions-*eg.*, ash or soot particles in fossil fuel (oil or coal-) combustion products, can acquire a sufficient fraction of this solid material to cause a noticeable decline in heat transfer performance. This decline is associated with the local growth of microgranular insulating 'fouling' layers,creating the need for periodic shutdown for cleaning. To predict required maintainance intervals for a particular (class of) fuel(s) and/or assess the most economical degree of fuel 'cleaning', a quantitative understanding of heat exchanger *fouling rates* is clearly necessary. From the viewpoint of capturing a non-negligible fraction of the mainstream particle flow rate *inertial impaction* is the mechanism responsible for most of the deposited mass and volume. However, by far the greatest uncertainty in making fouling rate predictions is associated with the appropriate single impacting particle *capture fraction* , or sticking probability s which, in general, is
a function of both incident velocity and angle but not yet fully understood for particle impaction on a granular deposit (Konstandopoulos (1991), Rosner *et al* (1992). In the present program we have

*For a review of multi-component convective-diffusion and thermophoretic particle mass transfer in chemically reactive flow systems, see, *e.g.*, Rosner, 1986,1990. Our prior experimental and theoretical studies of alkali *vapor deposition* are conveniently summarized in *J. PhysicoChemical Hydrodynamics* (Pergamon) **10**, [5/6], 663-674 (1988). For a useful overview of heat exchanger fouling research as of *ca.* 1989, see: Marner (1990).

also extended/applied *inertial impaction* theory (Konstandopoulos (1991), Rosner *et al* (1992)) and applied what we now know about *single particle capture behavior* (Konstandopoulos(1991) , Rosner *et al* (1992)) to predict the sensitivity of deposition rate to system parameters (*eg.*, mainstream velocity, particle mass loading, rebound velocity, mean particle size, tube diameter, *etc.* This capability could clearly be used to motivate, evaluate and implement "ruggedization" and/or *fouling reduction strategies.*

2. RESEARCH ACCOMPLISHMENTS AT THE YALE-HTCRE LAB

2.1 Prediction of Particle Deposition Rates in Engineering Equipment

Rosner and Tandon (1994) have developed a convenient formalism for making rational engineering predictions of deposition rates in high-gas velocity particle-laden environments, based, in part, on recently developed single particle sticking capture laws (Konstandopoulos (1991); Rosner *et al* (1992)) for impaction on granular deposits. Exploiting such information, even when available for the particular materials combinations of interest, to anticipate deposition rates in realistic engineering environments is normally a computationally demanding task since it is necessary to track the impingement frequency, velocity and incidence angles of all the different size particles in the mainstream capable of striking the target locations of interest, invoking the abovementioned *sticking (or 'rebound') laws* at each such point to predict the corresponding cumulative local deposition rate. However, by focusing our attention on the canonical geometry of a circular-cylindrical target in cross-flow (Fig.1) and introducing a modest number of defensible approximations (Section 2.2) to summarize the predicted and measured deposition rates on the solid surface of interest, we have shown that the tedious portion of such deposition rate predictions can be carried out 'once-and-for-all', thereby reducing the engineering problem of predicting target deposition rates, and the associated reduction in convective heat transfer rate, to that of multiplying a readily calculated *reference deposition rate* by a set of 'universal' dimensionless deposition rate functions calculated and reported here. Our reference deposition rate is that which would be expected in the prevailing environment if all the mainstream particles had the mean size and were captured upon impacting the target surface. For convenience, our results will be cast in terms of the following dimensionless parameters: ratio of mainstream velocity to the critical velocity for particle rebound from the solid surface, ratio of mean abrasive particle size to the threshold size required for impaction on the circular-cylinder target in the prevailing flow environment, spread of the mainstream particle size distribution (here assumed 'log-normal'), and the characteristic 'slip' Reynolds number for the critical size particles in the mainstream. In this way we have shown that many previously observed characteristics of fouling layers, including their frequently "lobular" appearance (Fig. 3), can be understood theoretically . Conversely, our procedure could be 'inverted', if necessary, to make preliminary estimates of single particle capture behavior based on deposition rate measurements made on a test circular cylinder in crossflow.

2.2 Principal Assumptions and Cases Explicitly Considered

To incorporate the essential phenomena in a simple manner without making unrealistic idealizations we have made the following basic assumptions:

A1 Local particle impaction frequencies, velocities, and angle-of-incidence can be calculated with sufficient accuracy from recently available correlations summarizing the results of individual suspended non-Brownian particle trajectories calculated for steady, inviscid flow past an isolated circular cylinder target , including non-Stokesian drag corrections (*cf.* Israel and Rosner, 1983) (Fig. 1)

A2 Even for impaction on granular deposits, single particle capture probability laws at particular velocities and incidence angles can be invoked to predict average deposition rates in engineering applications where suspended particles of different size arrive over a broad range of impact velocities and incidence angles.

A3. 'Rebounding' particles donot appreciably influence incoming particles, nor deposit in appreciable numbers upon re-impaction on the same target

A4 Predicted 'initial' deposition rate trends (spatial distributions) determined on an initially smooth circular

cylinder target can be used to anticipate longer time deposition trends on inevitably roughened cylinders which ultimately depart from circular shape due to localized deposit growth.

A5 The mainstream population of suspended particles is approximately log-normal with respect to particle volume and, while the particle *mass loading*, ω_p, in the mainstream may not be very small, the *volume fraction*, ϕ_p, corresponding to the total particle number density N_p and mean particle volume $\bar{v}$ (*ie*, $\phi_p = N_p \bar{v}$) *is* negligible.

Subject to these assumptions, we have shown that actual local deposition rates at position θ (Fig 1) can be expressed as the product of an easily calculated *reference deposition rate*, $(DR)_{ref}$, and a universal dimensionless function $D(\theta,...)$ introduced, calculated(Section 2.2) and plotted (Fig. 3) over the interesting range of mean suspended particle diameter (expressed as a multiple of critical diameter required for inertial impaction in the prevailing environment) and a dimensionless velocity ratio characterizing the rebound behavior of the particles on the surface of interest. An attractive feature of this formulation is that D, and its average value* $\bar{D}$, can be calculated 'once-and-for-all' *via* straightforward numerical quadratures in terms of an acceptably small number of dimensionless parameters defining the system (application). We have shown (Rosner and Tandon,1994) that the availability of these results dramatically simplifies the task of predicting local and total deposition rates for, say, heat exchanger tubes in the cross-flow of ash-laden combustion products . Moreover, by introducing a modified (heat transfer coefficient-weighted-) average value of $\bar{D}$, designated $\bar{D}_h$ (Fig.4), we also dramatically simplify the prediction of the associated *convective heat transfer reduction.*

2.3 Single Particle Capture Probability Laws and the Calculation of $D(\theta,...)$

In this work we have *applied* the micromechanical theory of particle *capture sticking fraction*, *s* (which provides the functional form of *s* when particular projectile particles are directed at particular target materials (including granular deposits) at a known velocity V_p and angle of incidence θ_i (*cf.* the target outward normal) to predict local and total particle capture rates for a cylindrical target immersed in a polydispersed suspension of such particulates. We considered three distinct classes of single particle capture laws, as follows: constant capture fraction, "on-off" (Fig.2a) capture behavior (expected on a 'clean' (particle-free) smoothe surface), and capture by a 'granular' deposit (above the particle critical velocity, the sticking probability does not fall abruptly to zero but , rather, exhibits an exponential 'tail' (see Fig. 2b).

The *dimensionless* local deposition rate function $D(\theta)$ is explicitly given by the integral:

$$D(\theta) = \frac{1}{\bar{v}} \cdot \int_0^\infty s(v,\theta) \cdot \eta_{local}(v,\theta) \cdot v \cdot C_\infty(v) \cdot dv \qquad (1)$$

To complete the calculation of $D(\theta,...)$ (see, *eg.*, Fig. 3) we specify the three inertial impaction functions: impact velocity:$V_p(v,\theta)/U$, angle-of-incidence (Fig.1) $\theta_i(v,\theta)$ and the local dimensionless impingement frequency $\eta_{local}(v,\theta)$. Our primary goal has been the mean value $\bar{D}$ of D over the upwind-facing surface of the circular cylinder*.

*It is interesting to note that $\bar{D}$ so defined is merely $(2/\pi)$ times the conventionally defined *total capture (efficiency) fraction*, η_{cap} based on target 'frontal area' Rosner (1986, 1990).

2.4 Associated Reduction in Convective Heat Transfer Rate

Because the principal reason for interest in deposition dynamics is the consequence of even a thin deposit for *heat transfer* performance, we have derived the following interesting explicit relation between fractional convective heat transfer reduction* and our local deposition rate predictions.An important result of this derivation is the relevance of the ($Nu_h(\theta)$-'weighted'-) integral:

$$\bar{D}_h \equiv \frac{2}{\pi}\cdot\int_0^{\pi/2} [\ Nu_h(\theta) / Nu_h(0)\ ] \cdot D(\theta,...)\cdot d\theta \qquad (2)$$

where the integrand contains tne angular (position) dependence of the local convective heat transfer coefficient. The relevance of $\bar{D}_h$ to heat transfer reduction is clearly understood when it is recognized that equal thickness deposits will have greater effect on convective heat transfer if located near the forward stagnation point region (where $Nu_h(\theta;Re)$ maximizes in the Re-range of interest) than if located near $\theta=\pi/2$ radians (*cf.* Figs. 1,3). We find that the *fractional reduction of convective heat transfer rate* $\dot{q}'$ with time t on stream is given by:

$$\frac{-\Delta\dot{q}'_w}{(\dot{q}'_w)_{t=0}} \equiv \frac{1}{1-\langle\varepsilon\rangle}\cdot\frac{(DR)_{ref}\,t}{d_t}\cdot\frac{k_g}{k_{dep}}\cdot\left[\frac{\frac{1}{2}Nu_h(0)}{\overline{Nu_h}}\right]\cdot\bar{D}_h \qquad (3)$$

To summarize, our 'universal' results for $D(\theta)$ and $\bar{D}_h$, coupled with Eq.(3) and a rational estimate of $(1-\langle\varepsilon\rangle)\cdot k_{dep}$ appropriate to the 'ash' deposit in question, could be used to predict the time-on-stream corresponding to, say, a fractional loss of convective heat transfer rate of $-\Delta\dot{q}'_w/\dot{q}'_w$ (10% , say). Under conditions where the deposits are not necesarily confined to the forward stagnation region (*eg.*, for impact/rebound on a bare surface at large values of $\bar{v}/v_{crit})^{1/3}$and $U/V_{p,cr}$, then $\bar{D}_h$ is found to be noticeably smaller than $\bar{D}$.

Figure 3 is a representative polar plot of dimensionless deposition rates on the upwind surfaces of the cylinder in crossflow for one of the sticking laws considered (Fig. 2). The rebound parameter ($U/V_{cr}(v_{cr}$ is only 0.1 for the case (shown) of capture on clean solid surfaces. The calculated contours are for different values of dimensionless mean volume, $\bar{\xi}$, defined as the ratio of $\bar{v}$ of the mainstream distribution and the critical particle volume, v_{crit}. For the case of capture on clean solid surfaces, an impacting particle is captured only if the normal velocity component, $V_{p,n}$, is less than the size-dependent critical velocity, $V_{p,crit}(v)$. Therefore, as the dimensionless mean size of the particles increases, a large fraction of these particles rebound in the forward stagnation region but somewhat smaller particles are captured at larger angles, θ, leading to the formation of deposits with off-axis 'lobes' (Fig. 3), which *have* been frequently observed.

Figure 4 summarizes representative results for the function $\bar{D}_h$ needed to predict *convective heat transfer reductions* (*via* Eq(3)). Trends for $\bar{D}_h$ are the same as those for $\bar{D}$ but, as expected, there is a systematic decrease below $\bar{D}$ in those cases for which there is appreciable off-axis deposition.

As shown in Rosner and Tandon (1994),a valuable byproduct of the present approach is the ability to evaluate the local *sensitivity* of deposition rates to key system parameters, such as gas velocity, mean particle size in the mainstream and target diameter. Our results indicate the presence of interesting opposing tendencies----for example, an increase in gas velocity increases the particle impingement rate but also increases the fraction of impacts leading to *rebound*. Similarly, an increase in target diameter would reduce the frequency of impacts but increase the likelihood of capture upon each (lower velocity) impact. It is clear that an understanding of these 'tradeoffs' will be necessary to evaluate the efficacy of rival strategies for reducing heat exchanger fouling rates.

3. CONCLUSIONS AND PLANS

In closing, we remind the practically-minded reader that it should be possible to embrace even phenomena which appear to be (explicitly) missing from our present analysis (*eg.*, larger particle capture effects associated with the simultaneous presence and capture of condensible *vapor* and/or *submicron* (subcritical) *particles* (see, *eg.*, Rosner and Nagarajan (1987), Rosner, Günes and Anous (1983)). For example, we would expect systematic shifts in the critical velocity for particle rebound, $V_{p,crit}(v)$, based on the relative amount of vapor and/or sub-micron (supercritical) particle deposition. We propose that several of these more complex but often-encountered situations be dealt with in future extensions and applications of the present 'baseline' analysis.

In comparing such deposition rate predictions with experiments, it should be borne in mind that, for 'thick' granular deposits, the preliminary methods emphasized here donot yet incorporate information on the *microstructure* and, hence, the void fraction of such deposits (see, *eg.*, Tassopoulos, O'Brien and Rosner, Tassopoulos and Rosner (1988)). Thus, we know from our ancillary studies that the local deposit *thickness* and associated local *thermal resistance* at any given time on-stream are not determined only by the history of the local particle volume fluxes due to impaction/capture.

Despite formidable complexities that remain to be overcome in the design and operation of power plants utilizing a broad spectrum of ash-bearing fuels, these recent methods and results are indicative of the potentially useful simplifications and generalizations emerging from our current fundamental research studies of suspended particle deposition mechanisms and their connection to microparticulate deposit formation. Our long-range investigations should continue in each of the underlying theoretical areas summarized above, as well as others beyond the scope of this brief report (see, eg., Rosner *et.al.*(1992)). Our goal is to provide engineering designers with significantly better "tools" for making rational assessments of ash deposition phenomena in future, high-performance coal-fired equipment. It is hoped that this invited PUEC review will accelerate this process *via* the requisite and timely exchange of R&D information among DOE contractors.

4. RELEVANT LITERATURE: DEPOSITION RATE FUNDAMENTALS

Castillo, J.L. and Rosner, D.E., "Theory of Surface Deposition from a Binary Dilute Vapor-Containing Stream, Allowing for Equilibrium Condensation within the Laminar Boundary Layer", *Int. J. Multiphase Flow*, **15**, [1], 97-118 (1989)

Castillo, J.L., and Rosner, D.E. "Non-equilibrium Theory of Surface Deposition from Particle-Laden, Dilute Condensible Vapor -Containing Streams, Allowing for Particle Thermophoresis and Vapor Scavenging within the Laminar Boundary Layer", *Int. J. Multiphase Flow*, **14** (1), pp. 99-120(1988)

Castillo, J.L., Garcia-Ybarra, P. and Rosner, D.E., "Morphological Instability of a Thermophoretically Growing Deposit", *J. Crystal Growth* **116**, 105-126,(1991)

Castillo, J.L., Mackowski, D.W., and Rosner, D.E., "Photophoretic Contribution to the Transport of Absorbing Particles Across Combustion Gas Boundary Layers", ACS Symposium Issue: **Ash Deposition**, *Prog. Energy and Comb. Sci.* **16**, 253-260 (1989)

Fernandez de la Mora, J., and Rosner, D.E.,"Inertial Deposition of Particles Revisited and Extended: Eulerian Approach to a Traditionally Lagrangian Problem", *J. Physicochemical Hydrodynamics (PCH)* (Pergamon) **2**, 1-21 (1981); see, also *J. Fluid Mech* **125**, 379-395 (1982)

Gokoglu, S. A and D. E. Rosner, "Note on the 'Windward Fraction' for Flow Past a Circular Cylinder", *Aerosol Sci. and Tech.*, **2** (4), 543-544 (1983)

Israel, R. and D. E. Rosner, "Use of Generalized Stokes Number to Determine the Aerodynamic Capture Efficiency of Non-Stokesian Particles from a Compressible Gas Flow", *Aerosol Sci. Tech.*, **2**, 45-51 (1983)

Gomez, A. and Rosner D. E. (1991) "Thermophoretic Effects on Particles in Counterflow Laminar Diffusion Flames", *Comb. Sci. Tech.* **89** 335-362 (1993)

Israel, R. and D. E. Rosner, "Use of Generalized Stokes Number to Determine the Aerodynamic Capture Efficiency of Non-Stokesian Particles from a Compressible Gas Flow", *Aerosol Sci. Tech.*, **2**, 45-51 (1983)

Konstandopoulos, A.G., and Rosner, D.E., "Experimental and Theoretical Studies of the Combined Effects of Particle Inertia and Thermophoresis on Deposition Rates Across Laminar Combustion Gas Boundary Layers" *Int. J. Heat Mass Transfer* (in press,1994)

Konstandopoulos, A.G., Labowsky, M.J. and Rosner, D.E.,"Inertial Deposition of Particles from Potential Flows Past Cylinder Arrays" *J. Aerosol Science* (Pergamon) **24** (4) 471-483 (1993)

Konstandopoulos, A. G. "A Micro-Mechanical Approach to Particle Capture and Deposit Growth" (Ch.5, PhD Dissertation: **Effects of Particle Inertia on Aerosol Transport and Deposit Growth Dynamics**, Yale University ChE, ME Depts. (1991)

Konstandopoulos, A. G. and Tassopoulos, M. "A Kinetic Model for Deposit Growth. Part I: Characterization of Sticking Probabilities",*AAAR 1990 Annual Meeting*, Paper 6E.6, June 18-22, 1990, Philadelphia, PA. .

Konstandopoulos, A. G., Labowsky, M. J. and Rosner, D. E. , "Inertial Deposition of Particles from Potential Flows Past Cylinder Arrays", *J. Aerosol Sci.*, **24** (4), 471-483(1993)

Liang B., Gomez, A., Castillo J. and Rosner D.E., "Experimental Studies of Nucleation Phenomena within Thermal Boundary Layers — Influence on Chemical Vapor Deposition Rate Processes", *Chem. Engrg Communications* **85**,113-133 (1989)

Marner, W.J.,"Progress in Gas-Side Fouling of Heat Exchanger Surfaces", in **Proc. A.L. London Symposium on Compact Heat Exchangers**, pp 421-489, Hemisphere, Washington DC.(1989); also available as: ASME Book # AMR069 or *Appl. Mech Rev* **43** (3), 35-66 March (1990)

Park, H. M. and Rosner D. E., "Combined Inertial and Thermophoretic Effects on Particle Deposition Rates in Highly Loaded Dusty Gas Systems", *Chem. Eng. Sci.*, **44** (10), 2233-2244 (1989)

Rosner, D.E., "Total Mass Deposition Rates from 'Polydispersed' Aerosols"; *AIChE J.* **35**, [1], 164-167 (1989)

Rosner D.E. and Tassopoulos M., "Mass Deposition Rates from Streams Containing 'Polydispersed' Particle Populations of Arbitrary Spread", *AIChE J.* **35** (9) 1497-1508 (1989)

Rosner, D.E., "Experimental and Theoretical Research on the Deposition Dynamics of Inorganic Compounds from Combustion Gases"; Invited paper,*B. G. Levich Memorial Issue of J. PhysicoChemical Hydrodynamics*(PCH) (Pergamon) **10**, [5/6], 663-674 (1988)

Rosner, D. E. and Kim, S. S. "Optical Experiments on Thermophoretically Augmented Submicron Particle Deposition from 'Dusty' High Temperature Gas Flows", *Chem. Engng. J.*, **29**, pp. 147-157 (1984).

Rosner, D.E., and Nagarajan, R., "Toward a Mechanistic Theory of Deposit Growth from Ash-Laden Flowing Combustion Gases: Self-Regulated Sticking of Impacting Particles and Deposit Erosion in the Presence of Vapor 'Glue'", in *AIChE Symposium Series*, **83**, No. 257, **Heat Transfer-Pittsburgh 1987** (R.W. Lyczkowski, ed.) 289-296 (1987)

Rosner, D.E., Mackowski, D.W., and Garcia-Ybarra, P., "Size- and Structure-Insensitivity of the Thermophoretic Transport of Aggregated 'Soot' Particles in Gases", *Combustion Science and Technology* **80**,(1-3),87-101(1991)

Rosner, D.E., Mackowski, D.W., Tassopoulos, M., Castillo, J., Garcia-Ybarra, P., "Effects of Heat Transfer on the Dynamics and Transport of Small Particles Suspended in Gases", *Ind/Engrg. Chem-Res* (ACS) **31**,760-769 (1992)

Rosner, D.E. and Tandon, P., "Rational Prediction of Inertially-Induced Particle Deposition Rates on a Cylindrical Target in Dust-Laden Streams: Effects of Single-Particle Capture Law and Dust Polydispersity on Deposition Rates and Associated Convective Heat Transfer Reductions" , HTCRE Paper No. 202 , March 1994

Rosner, D.E., Konstandopoulos, A., Tassopoulos, M. and Mackowski, D.W., "Deposition Dynamics of Combustion-Generated Particles: Summary of Recent Studies of Particle Transport Mechanisms, Capture Rates and Resulting Deposit Microstructure/Properties", in **Inorganic Transformations and Ash Deposition During Combustion**, (S.A.Benson, ed)., Engineering Foundation/ASME, (1992); pp 585-606

Rosner, D.E.*et. al.*, "Research on Fundamental Aspects of Inorganic Vapor and Particle Deposition in Coal-Fired Equipment", *Proc.* 7th, 8th, 9th *Annual DOE-PETC Coal PUEC Contractor's Meetings*, July 1991,1992,1993 (respectively), Pittsburgh, PA.

Rosner, D. E. and Fernandez de la Mora J. , "Correlation and Prediction of Thermophoretic and Inertial Effects of Particulate Deposition from Non-Isothermal Turbulent Boundary Layers", in **Particulate Laden Flows in Turbomachinery**, W. Tabakoff, C. T. Crowe and D. B. Cale, eds., ASME, NY, 85-94 (1982)

Rosner, D. E. and Fernandez de la Mora J. , "Boundary Layer Effects on Particle Impaction and Capture", *ASME Trans.--J. Fluid Engrg.*, **106**, 113-114 (1984)

Rosner, D. E., Günes D., and Anous N. , "Aerodynamically-Driven Condensate Layer Thickness Distributions on Isothermal Cylindrical Surfaces", *Chem. Engrg. Comm.*, **24**, 275-287 (1983)

Rosner, D. E., Gökoglu, S. and Israel, R., "Rational Engineering Correlations of Diffusional and Inertial Particle Deposition Behavior in Non-Isothermal Forced Convection Environments", in **Fouling and Heat Exchanger Surfaces**, Engrg. Foundation, NY, 235-256 (1983)

Rosner, D. E., **Transport Processes in Chemically Reacting Flow Systems**, Butterworth-Heinemann Publishers, Stoneham, MA (1986); 3d Printing Dec 1990, 4th Printing (Contact Author Directly)

Rosner, D. E., A. G. Konstandopoulos, M. Tassopoulos and D. W. Mackowski, "Deposition Dynamics of Combustion Generated Particles: Summary of Recent Studies of Particle Transport Mechanisms, Capture Rates and Resulting Deposit Microstructure / Properties", Proc. Engrg.Fndtn. Conf., **Inorganic Transformations and Ash Deposition During Combustion**, ASME Enrgr. Foundation, 585-606 (1992)

Rosner, D.E. and Atkins, R.M., "Experimental Studies of Salt/Ash Deposition Rates from Combustion Products Using Optical Techniques", in **Fouling and Slagging Resulting From Impurities in Combustion Gases** (Bryers, R. W., ed.), Engineering Foundation, NYC, Publication No. 81-18 (1983), pp.469-492; in particular: Rosner, D.E., Appendix: "Recent Advances in the Theory of Deposition From Combustion Gases", pp. 486-492

Tassopoulos, M., **Relationships Between Particle Deposition Mechanism and Resulting Deposit Microstructure/Effective Transport Properties**, PhD Dissertation, Yale University, Dept. ChE (1991)

Tassopoulos, M. and Konstandopoulos, A. G. "A Kinetic Model for Deposit Growth. Part II: Characterization of Microstructure and Transport Properties" *AAAR 1990 Annual Meeting*, Paper 6E.6, June 1990, Philadelphia, PA.

Tassopoulos, M. and Rosner, D.E., "Simulation of Vapor Diffusion in Anisotropic Particulate Deposits", *Chem. Eng. Sci.* **47**(2) 421-443 (1991)

Tassopoulos, M. and Rosner, D.E.,"The Effective Thermal Conductivity of Anisotropic Packings of Spheres" (Part 1."Conduction Through the Solid Phase"; Part 2."Conduction Through the Solid and Void Phases"),*Chem. Eng. Sci.* (in press(1994))

Tassopoulos, M. and Rosner, D.E., "Microstructural Descriptors Characterizing Granular Deposits", *AIChE J.* **38**(1) 15-25 (1991)

Tassopoulos, M., O' Brien,J. A. and Rosner D .E., "Simulation of Microstructure-Mechanism Relationships in Particle Deposition, *AIChE J.* **35** (6) 967-980 (1988)

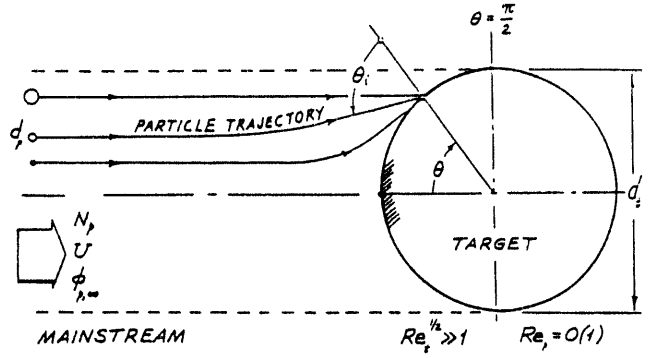

Fig. 1 Fouling of a heat exchanger surface (cylinder in high Reynolds number crossflow) in response to the arrival of impacting particles log-normally distributed with respect to size. Particle *capture fraction s* taken to be dependent on incident velocity (Fig. 2) and angle θ_i .

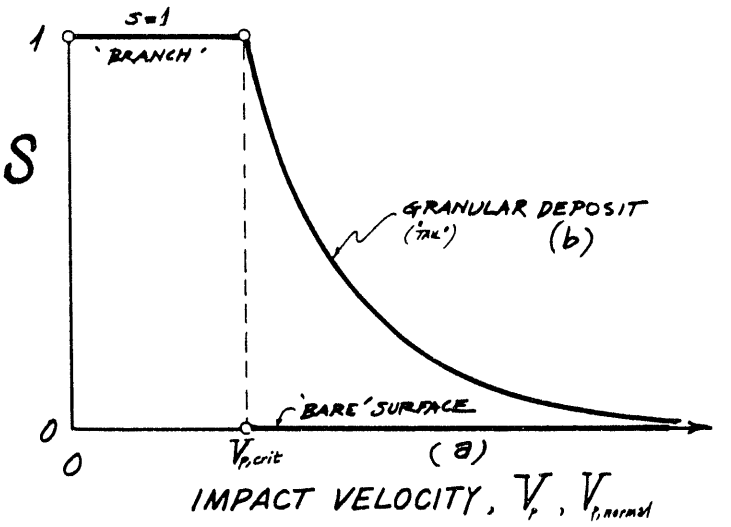

Fig. 2 Single particle *capture probability laws* (particle velocity dependence) considered (Rosner and Tandon, 1994). Cases shown: capture on a clean solid surface; and incident particle capture by a *granular deposit* (after Konstandopoulos,1992)

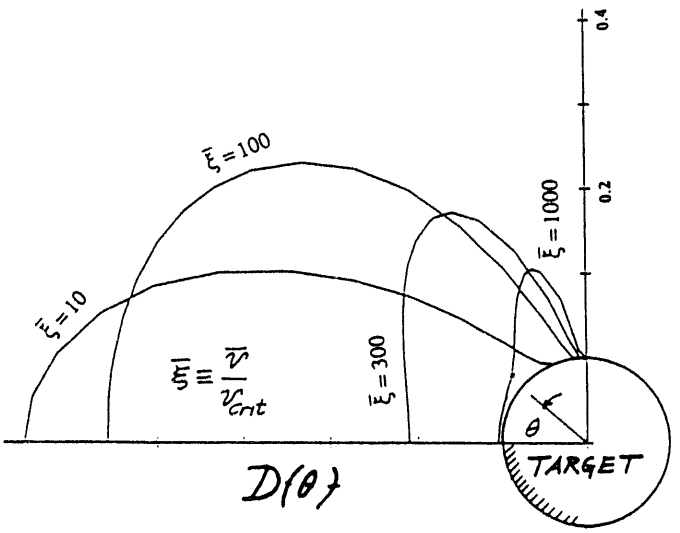

Fig. 3 Polar plot of the local dimensionless *deposition rate* for several values of the particle population size parameter $\bar{v}/v_{crit}$; Cases shown: Threshold velocity for critical size particle *rebound* equal to ten times the mainstream velocity, U (after Rosner and Tandon, 1994).

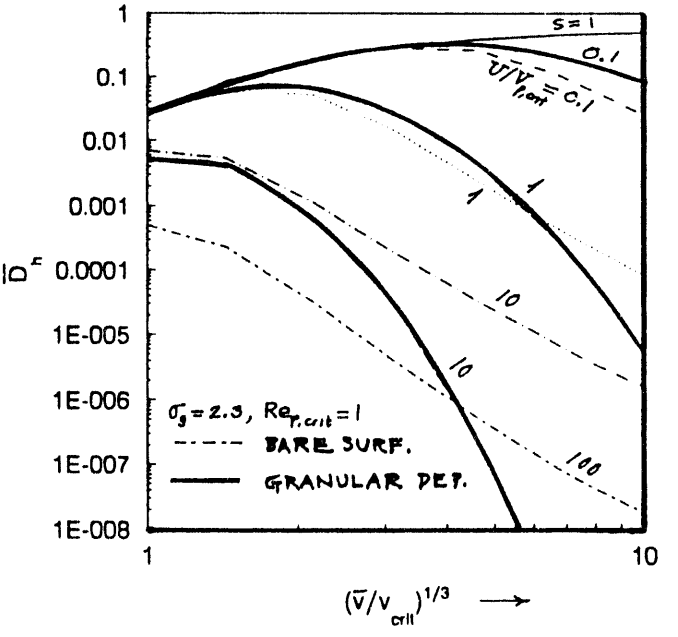

Fig. 4 Upwind surface-averaged deposition rate function dictating convective *heat transfer reductions* (*via* Eq. 3). Dependence on mean particle size (volume) in the mainstream population for each class of particle sticking fraction law (Fig. 2). (after Tandon and Rosner, 1994)

RECENT PROGRESS IN THE USE OF SYNCHROTRON RADIATION

FOR THE ANALYSIS OF COAL COMBUSTION PRODUCTS

B. MANOWITZ*, S. G. KANG**, L. BOOL**, J. J. HELBLE**,
N. SHAH***, AND G. P. HUFFMAN***

*BROOKHAVEN NATIONAL LABORATORY, UPTON, NEW YORK 11973
**PSIT TECHNOLOGY COMPANY, ANDOVER, MASSACHUSETTS 01810
***UNIVERSITY OF KENTUCKY, LEXINGTON, KENTUCKY 40506

Contract Number: AS-227-APD

Period of Performance: 1 October 1988 - Open

Introduction

The formation and build-up of slag deposits on heat transfer surfaces is one of the most serious problems in pulverized coal combustion. This phenomenon, traditionally called wall slagging, is known to cause undesirable effects on heat and mass transfer and in some instances induce corrosion. Many empirical formulations based on silica percentage and acid/base ratio have been developed in the past to describe the slag characteristics. Unfortunately, due to variation of several factors such as flame turbulence, residence time, temperature distribution, gas velocity variance, etc. within the boiler, these empirical formulations are of limited use in the prediction of the behavior of the slag. Of even more importance, these formulations do not take into account the interaction of the coal constituents within and immediately after the flame.

What is believed to be a major mechanism for the production of slag is the formation of low melting eutectic compounds in the post combustion region, many of which will stick to the heat transfer surface. The composition of this slag may very well change during operation as layers of the slaggy material build up or break off.

An understanding of the chemical composition of such slags under boiler operating conditions and as a function of the mineral composition of various coals is the ultimate goal of this program.

The principal constituents in the ash of many coals are the oxides of Si, Al, Fe, Ca, K, S, and Na. The analytical method required must be able to determine the functional forms of all of these elements both in coal and in coal ash at elevated temperatures. One unique way of conducting these analyses is by x-ray spectroscopy.

The Extended X-Ray Absorption Fine Structure (EXAFS) and X-Ray Absorption Near Edge Structure (XANES) spectroscopic techniques and other applications to the chemical speciation of coal combustion products have been described previously.[1] Therefore only a short summary will be included here. The experiment involves scanning through the K- or L-shell absorption edge of the element in question. The structure of the absorption edge, consisting of transitions to unoccupied molecular levels, can be compared to those of model compounds for identification. The relative position of the absorption edge can yield information regarding the oxidation state of the element. This portion is the XANES portion of the spectrum. The EXAFS region, extending from about 60 eV above the absorption edge, represents scattering from neighboring constituents and can be used to determine the coordination number and coordination distance of a specific element from its neighboring atoms.

The best source of excitation energy for these experiments is an electron storage ring emitting synchrotron radiation (SR).[2] The National Synchrotron Light Source (NSLS) at Brookhaven National Laboratory is a 2.5-GeV storage ring and emits a continuous spectrum of x rays to an energy of about 30 keV. Beam line X-19A is dedicated to XANES and EXAFS and is being adapted to the performance of this investigation.

The program involves a combined effort between the staff of the University of Kentucky, PSI Technology, Inc., and Brookhaven National Laboratory. The principal recent effort has been the design, construction, testing, and operation of an *in-situ* combustion cell.

Analysis of Iron Compounds

The chemical state of iron compounds has a significant effect on their stickiness under coal combustion conditions. For example, the mineral pyrite is crystalline and relatively non-sticky. Similarly, crystalline magnetite and hematite, the end products of pyrite oxidation, are crystalline and non-sticky. Several intermediate products are molten, however. These include the sulfide pyrrhotite and its oxy-sulfide derivatives, which may be either molten or solid, depending upon temperature and extent of reaction.

During combustion, iron may also become incorporated into glassy aluminosilicate-derived ash particles. Because glassy particles are often sticky, these particles may also deposit on and adhere to available surfaces. In prior research conducted at PSI, particle stickiness has been shown to be a function of particle viscosity. Thus, knowledge of the precise composition of iron-containing glass particles is an important parameter in determining their viscosity and stickiness. In addition to composition, the oxidation state of iron-containing glasses must also be known. For iron dissolved in glass, the (+2) oxidation state results in a significantly lower viscosity than does the (+3) oxidation state.

To understand and eventually predict the deposition or iron-containing ash particles, it is therefore critical that the precise chemical state of iron at the point of encounter with an impaction surface be known. XAFS spectroscopy is one technique useful for determining the chemical speciation of iron. Typically XAFS spectroscopic analysis is conducted on a sample that has been quenched and removed from the combustion process. While this provides valuable insight into the possible states of iron, the possibility of quench-induced phase formation cannot be avoided.

In this program, an *in-situ* XAFS combustion furnace and measurement cell have been constructed by PSI, U. Kentucky, and DAS personnel to permit measurement of the forms of iron and other elements without the need for quenching and sample removal. This permits the state of iron to be measured in deposit samples as well as in flowing ash particle stream. Changes occurring over the duration of sampling--for example, oxidation of an oxysulfide sample sitting on a tube surface--can also be detected.

Use of the *in-situ* cell also permits the effect of combustion conditions on the forms of iron and other elements to be determined. For example, under staged reducing stoichiometries such as those associated with low-NO_x conditions, the oxidation rate of pyrite to magnetite will be slowed. This may result in a longer duration intermediate melt phase, in turn leading to increased deposition in a utility boiler.

Results of Furnace Runs

The *in-situ* combustion cell, designed to carry out *in-situ* XANES measurements of flyash particles as well as ash deposits, is comprised of mainly two systems: (i) the control system and (ii) the furnace system. The control system is contained in a cabinet on wheels and is composed of the gas control system, the interlock system and the furnace controller. The furnace system is composed

of the preheater, the diffuser, the coal feeder, the furnace, the six-way cross, the ash collection system, and the pump. The furnace system is separable into two sections each of which is on wheels and can be moved in and out of the hutch at beam line X-19A at the NSLS. Figure 1 shows a schematic diagram of the furnace system. A full description is given in Reference (3).

The premier run of the system is reported in Reference (3). This report summarizes the results of runs in August 1993 and in March 1994. The data are taken at a deposition probe simulating deposition at a heat transfer surface.

The following table indicates the experimental conditions for the *in-situ* experiments in our August 1993 run.

Sample	Feed Rate (g./min)	Furnace Temp. (°C)	% O_2	Substrate Temp. (°C)
Pyrite	1	1300	20	460
Pyrite	1	1300	14	520
Pyrite	1	1300	5	560
KY #9	2	1100	20	400
KY #9	4	1300	20	480
KY #9	4	1400	20	500
KY #9	6	1500	20	650
KY #9	6	1500	5	700

Pyrite Feed:

Figure 2 shows Fe K-edge XANES of deposit formed while pyrite was fed at 1 g./min feed rate to the furnace at 1300°C. The deposition probe temperature was about 460°C. Air was used for the primary air supply and for the pyrite feed stream. The initial deposit (bottom spectra in the figure) showed less oxidation as compared to the outer deposit (middle spectra). Pyrite feed was then stopped and hot air was allowed to pass over the deposit to monitor further transformations in the deposit. After two hours of "aging," the XANES spectra of the deposit did not indicate any further changes in the deposit.

Oxygen partial pressure was reduced to 5% by substituting nitrogen for feeder air and by mixing nitrogen with the primary air. The bottom spectra in figure 3 shows Fe XANES of the deposit collected at 1300°C furnace temperature and 5% oxygen partial pressure. Under reducing conditions, pyrite does not oxidize completely but forms what may be an Fe-oxysulfide phase. The pre-edge peak in the spectra indicates the onset of iron oxide phase formation. When the partial pressure of oxygen was increased to 14%, the pre-edge peak was better defined. In fact, the spectrum for 14% oxygen partial pressure is very similar to that collected at 20% oxygen partial pressure (see figure 2).

Kentucky #9 Coal Tailings Feed:

Feeder and feed line were emptied and cleaned to remove leftover pyrite and the feeder was replenished with utility grind Kentucky #9 coal tailings. Since the coal tailings have lower iron content than pyrite, the feed rate was increased and detector gains were optimized to improve the signal to noise ratio.

Figure 4 shows a series of XANES spectra collected at 20% oxygen partial pressure and at varying furnace temperature settings. The spectra are quite similar to each other, but show subtle differences in the pre-edge feature. The spectrum is also similar to that of the deposit obtained when pure pyrite was fed to the furnace.

Figure 5 is a comparison between XANES spectra obtained for Kentucky #9 coal tailings under oxidizing (20% O) and reducing (5% O) operating conditions at 1500°C furnace set point. Just like pure pyrite feed (figure 3), at lower oxygen partial pressures, iron does not completely oxidize but appears to be incorporated in an oxide-sulfide mixture. This phase is quite sticky and easily forms an initial deposit. During this experiment, a substantial amount of this highly viscous slag phase was deposited in the alumina retort and plugged up the ash stream concentrator at the bottom of the furnace. At longer residence times, even under reducing conditions, this slag transformed into a very tenacious deposit and was impossible to remove.

An *in-situ* combustion XAFS experiment was performed at the beam line X-19A of the NSLS during March 23-29 1994. The following is a summary of the results of the experiment.

Experimental Matrix

In order to achieve a uniform feed rate and to facilitate complete combustion, Pittsburgh #8 (Blackville #2) coal was sieved to < 75 μ size fraction and this fine fraction of coal was used for the combustion experiment.

The following experimental matrix was set up to observe the effect of variation in the stoichiometric ratios and temperatures on the ash deposit formation. The coal feed rate was maintained at one gram per minute for all experimental conditions. Though the furnace is designed to handle one SCFM gas flow, the flow rate was reduced to increase residence time and to achieve complete combustion. The output oxygen concentration was measured at one of the ports of the 6-way cross with an oxygen analyzer. The accuracy of the analyzer was reported to be ± 1%.

Stoichiometric Ratio (Calculated)	Total Gas Flow	Preheated Gas Flow		Feeder Gas Flow		Input O_2 Conc. (Calc.)	Output O_2 Conc. (Measured)
	SCFM	Air SCFM	N_2 SCFM	Air SCFM	N_2 SCFM	%	%
Furnace Temp. Setting - 1300°C							
2.45	0.75	0.6		0.15		21	15
0.9	0.5	0.27	0.03		0.2	11.5	5
0.7	0.5		0.3	0.2		9	3.2
Furnace Temp. Setting - 1400°C							
1.6	0.5	0.3		0.2		21	12.5
0.9	0.5	0.27	0.03		0.2	11.5	1
0.7	0.5		0.3	0.2		9	1.5

Pittsburgh #8 Feed

Figures 6 and 7 show Fe K-edge XANES of Pittsburgh #8 coal deposits obtained for furnace temperature settings of 1300 and 1400°C respectively. The coal feed rate was maintained at one g/min. The XANES spectra for all six of the conditions studied appear similar. The spectra indicate presence of iron oxide and iron in aluminosilicate glassy phase.

Several times during the experiment, we noticed an increase in the differential furnace pressure drop indicating a blockage to air flow. Usually, this was due to clogging of the Balston filter used as fine ash trap. Some char from this ash trap was analyzed later for carbon content. Even for the highest stoichiometric ratio (2.45) we noticed substantial (about 50%) carbon content in the ash. This suggests that the combustion is incomplete in all the cases and the combustion conditions remain reducing for all the cases. We have to increase residence time to force complete combustion and to truly achieve the desired stoichiometric ratios.

Discussion

The data are being further analyzed for journal publication. At this stage the results illustrate the feasibility of the technique for obtaining *in-situ* information on combustion ash deposition composition.

Acknowledgements

Research is supported by the Pittsburgh Energy Technology Center, US Department of Energy, under Contract No. DE-AC02-76CH00016.

References

1. A. Bianconi, "XANES spectroscopy," in X-Ray Absorption, D. C. Koningsberger and R. Prins, eds., Wiley and Sons, New York, 1988, pp. 573-661.
2. A. Winick, "Properties of synchrotron radiation," in Synchrotron Radiation Research, H. Winick and S. Doniach, eds., Plenum Press, New York, 1980, pp. 11-25.
3. B. Manowitz *et al.*, Proceedings of the Ninth Annual Coal Preparation, Utilization, and Environmental Control Contractors Conference, 1992, Pittsburgh, PA.

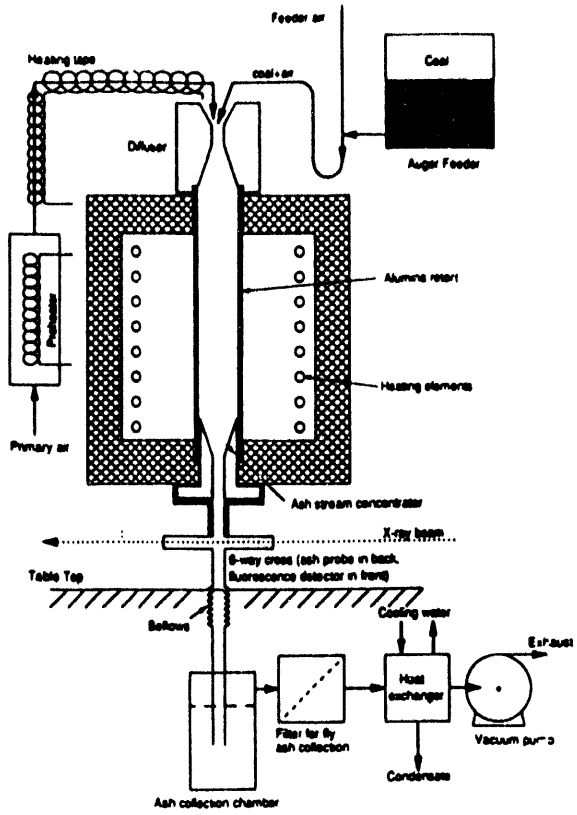

Figure 1. Schematic of *in-situ* XAFS furnace system.

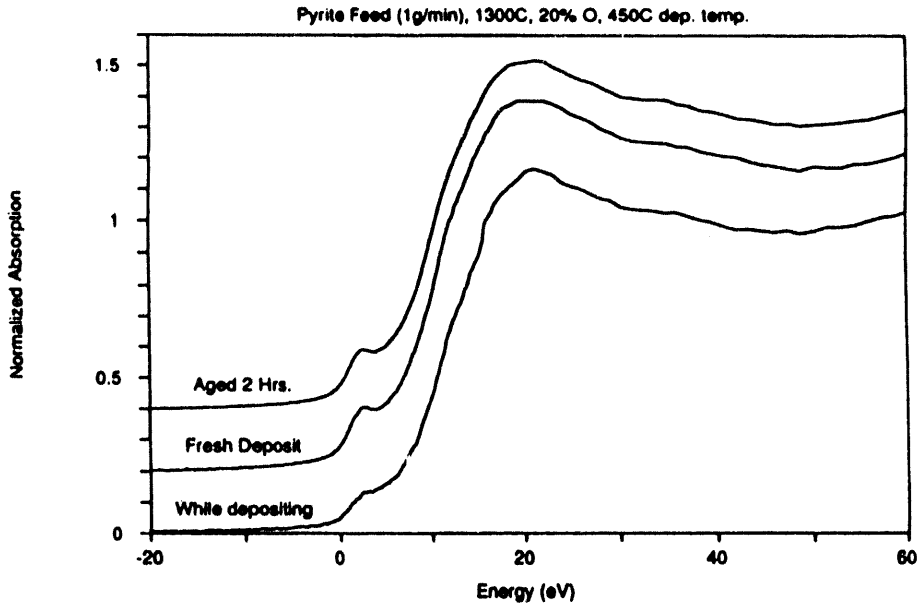

Figure 2. Fe K-edge XANES of *in-situ* pyrite deposit at 1300°C after varying exposure at combustion conditions.

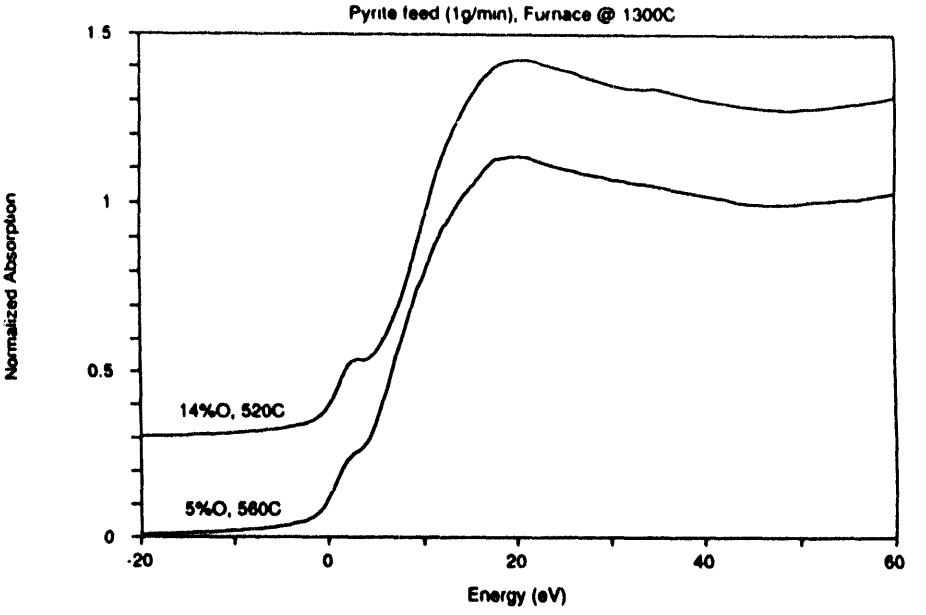

Figure 3. Fe K-edge XANES of *in-situ* deposits of pyrite at 1300°C under oxidizing and reducing conditions.

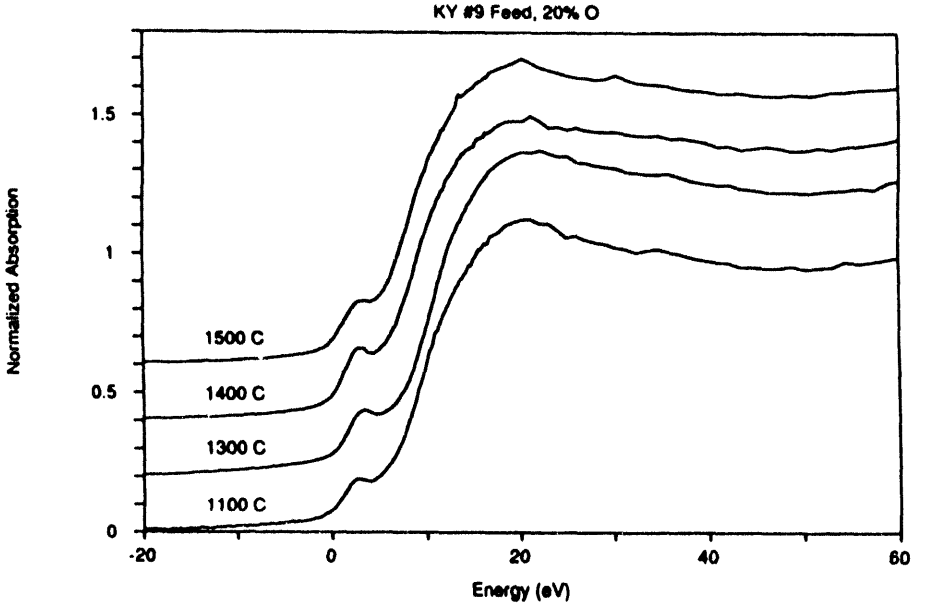

Figure 4. Fe K-edge XANES of *in-situ* deposit of Kentucky #9 coal at various furnace temperature settings (under oxidizing conditions).

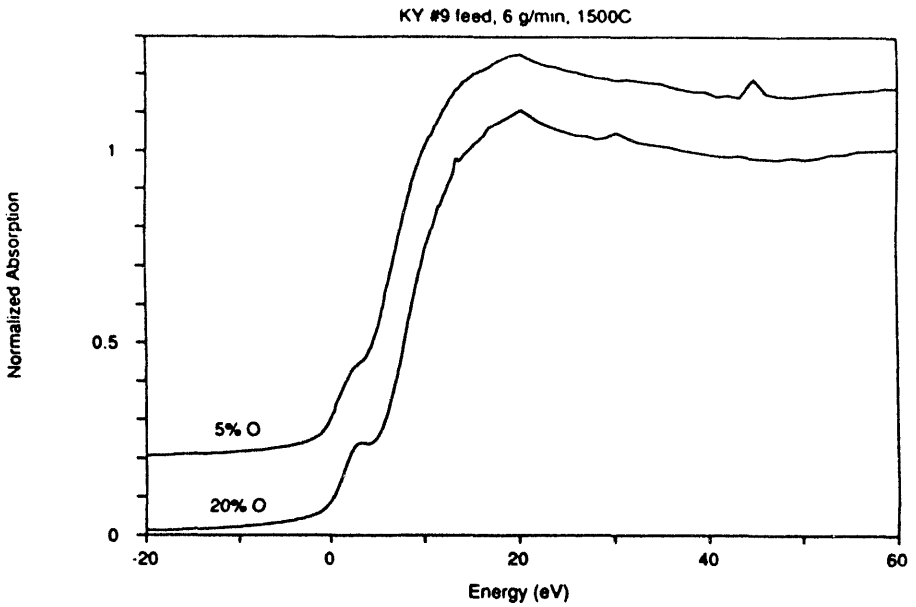

Figure 5. Fe K-edge XANES of *in-situ* deposit of Kentucky #9 coal at 1500°C under oxidizing and reducing conditions.

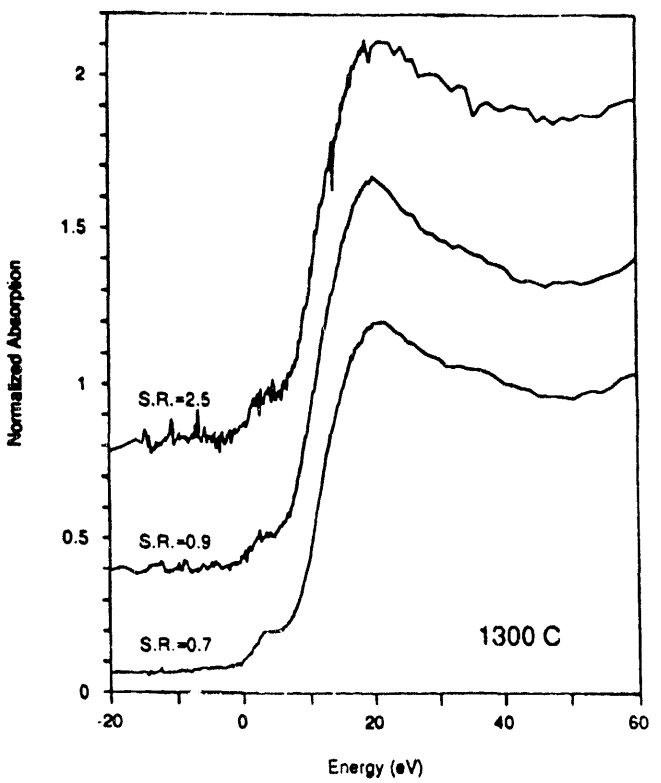

Figure 6. Fe K-edge XANES of Pittsburgh #8 coal deposits obtained at different stoichiometric ratios. 1 g/min coal feed rate at 1300°C furnace setting.

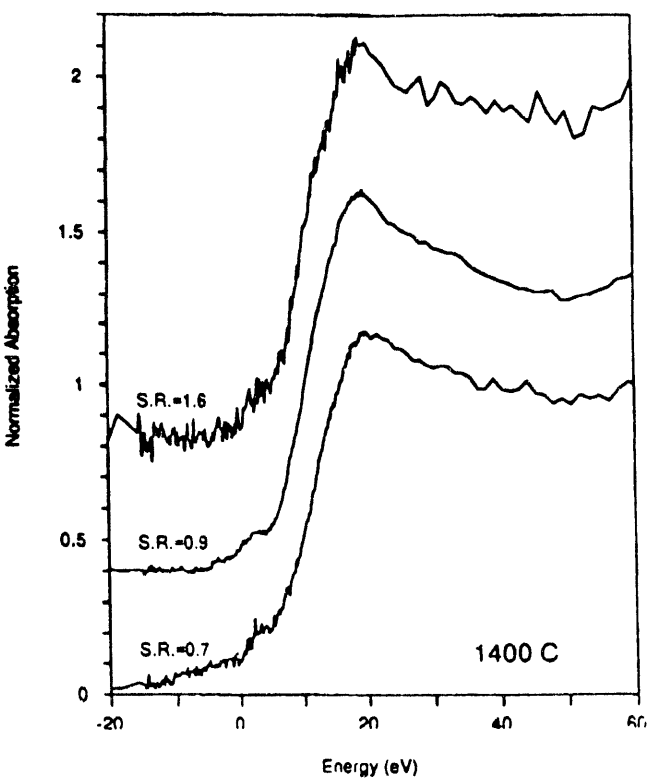

Figure 7. Fe K-edge XANES of Pittsburgh #8 coal deposits obtained at different stoichiometric ratios. 1 g/min coal feed rate at 1400°C furnace setting.

Fundamental Study of Ash Formation and Deposition: Effect of Reducing Stoichiometry

Dr. J.J. Helble, Dr. L.E. Bool, Dr. S.G. Kang, and Mr. G.A. Moniz
PSI PowerServe

Prof. A.F. Sarofim and Mr. T. Zeng
Massachusetts Institute of Technology

Prof. T.W. Peterson and Mr. D. Gallien
University of Arizona

Prof. G.P. Huffman and Prof. N. Shah
University of Kentucky

1. Objectives and Approach

This project is designed to examine the effects of combustion stoichiometry on the fundamental aspects of ash formation and ash deposit initiation. Emphasis is being placed on reducing stoichiometries associated with low-NOx combustion, although a range of oxidant/fuel ratios are being considered. Previous work has demonstrated that ash formation depends strongly upon coal mineralogy, including mineral type, size, amount, and the presence of organically associated inorganic species. Combustion temperature and the oxidation state of iron also play a significant role. As these latter items will vary with changes in stoichiometry, research to determine the net effect on deposition is required.

To achieve these goals, a research program with the following technical objectives is being pursued:

(1) identify the partitioning of inorganic coal constituents among vapor, submicron fume, and fly ash products generated from the combustion of pulverized coal under a variety of combustion stoichiometries.

(2) identify and quantify the fundamental processes by which the transformation of minerals and organically-associated inorganic species occurs. Identify any differences from standard excess air pulverized coal combustion conditions.

(3) modify, to incorporate the effects of combustion stoichiometry and based on the understanding developed in (1) and (2) above, an Engineering Model for Ash Formation. The previously developed model is capable of predicting the size and chemical composition distributions of the final ash products under standard pulverized coal combustion conditions of 20% excess air. These modifications will extend the model to include phenomena that may be dominant under a broad range of stoichiometries.

Experiments, sample analyses, and modeling are being conducted at several facilities as part of this program. Detailed coal and ash sample analysis using Mössbauer spectroscopy, X-ray absorption fine structure spectroscopy (XAFS), and computer controlled scanning electron microscopy are being carried out at the University of Kentucky (UKy). Small-scale drop tube combustion tests using size and density classified coal samples are being carried out at the Massachusetts Institute of Technology (MIT) to determine the extent of mineral coalescence and inorganic vaporization as a function of combustion stoichiometry. Combustion experiments utilizing utility grind coals are being conducted at PSI to examine the effects of stoichiometry on mineral interactions. Deposition experiments using ash generated from combustion experiments and using pure minerals are also being conducted to investigate deposit initiation as a function of combustion conditions. PSI's Engineering Model for Ash Formation (EMAF) is being modified to include effects of combustion stoichiometry as part of this effort. Self-sustained pilot scale combustion experiments are being conducted in the University of Arizona (UA) 100,000 Btu/h facility to address issues of scaling in combustion processes. The interaction of iron with aluminosilicates as a function of changing combustion conditions will be the focus of this effort. Modeling of iron-aluminosilicate interactions is being conducted as part of the UA study.

2. Coal Selection and Characterization

Four U.S. coals will be studied during this program: 1) Black Thunder sub-bituminous coal from the Powder River Basin, 2) a run-of-mine Pittsburgh #8 bituminous coal from the Appalachian Basin, 3) a washed commercial version of a Pittsburgh #8 coal obtained from DOE/PETC, and 4) a physically beneficiated product produced from Pittsburgh #8 coal. One additional coal may be obtained from Great Britain as part of a collaborative effort with a program led by the utility Powergen. Ultimate, proximate, and ash chemical analyses for the U.S. coals are reported in Table 1. CCSEM analyses are summarized in Table 2, and Mössbauer data are summarized in Table 3.

3. Effect of Carbon Content on Ash Particle Stickiness

One of the important questions to be answered in this work is the effect of sub-stoichiometric combustion conditions on ash deposition behavior. One of the effects of substoichiometric conditions is the presence of residual carbon and unoxidized, or only partially oxidized, pyrite in the ash. Experiments have been performed at PSI to explore the effect of these components on ash stickiness. These experiments focused on the stickiness of ash particles at short residence times. Although the experiments were all carried out under fuel lean conditions, the presence of carbon and partially oxidized pyrite in the ash at short residence times is similar to that obtained by combustion of the coal under reducing conditions.

For these experiments the coal, washed Pittsburgh No. 8 (DOE), was fed at 0.6 g/min into an entrained flow reactor described elsewhere (Helble et al., 1992). To control the fractional conversion of pyrite and the amount of carbon in the ash, the residence time was varied between 0.25 and 2.9 seconds by varying injection probe location and gas flowrates.

Table 1. Proximate, Ultimate, and Ash Analysis of Coals

	Pittsburgh #8 (Run-of-Mine)		Pittsburgh #8 (DOE)		Pittsburgh #8 (SCS Cleaned)		Black Thunder (UNDEERC)	
	As received	Moisture free	As-received	Moisture free	As-received	Moisture free	As-received	Moisture free
Proximate Analysis								
Moisture	2.00	-	1.40	-	2.00	-	24.30	-
Volatile Matter	30.76	31.40	36.85	37.36	36.37	37.13	35.89	47.42
Fixed Carbon	40.09	40.88	54.27	55.06	56.42	57.55	35.32	46.64
Ash	27.15	27.72	7.48	7.58	5.21	5.32	4.49	5.94
Ultimate Analysis								
C	57.16	58.35	77.05	78.11	77.22	78.83	52.84	69.83
H	4.00	3.86	4.79	4.70	5.51	5.39	7.04	5.73
N	0.98	1.00	1.39	1.41	1.37	1.40	0.70	0.92
O (ind)	8.43	6.76	7.40	6.27	8.98	7.33	34.54	17.07
S	2.28	2.32	1.89	1.92	1.71	1.74	0.39	0.51
Btu/lb	10,040	--	13,560	--	13,900	--	9,620	--
Ash Analysis								
SiO_2	54.82		46.81		42.7*		32.57	
Al_2O_3	23.06		25.03		25.2		16.81	
Fe_2O_3	10.52		14.76		20.8		5.69	
CaO	3.48		4.80		2.8		22.09	
MgO	2.26		1.71		1.0		4.79	
Na_2O	0.50		0.94		0.1		0.93	
K_2O	1.74		1.02		1.3		0.15	
TiO_2	0.87		0.72		1.4		1.11	
P_2O_5	0.13		0.19		0.4		1.17	
SO_3	2.63		4.02		2.6		14.69	

*Analysis of ABB/CE bulk sample.

Table 2. CCSEM Analysis of Program Coals (Wt%)

	Pittsburgh #8 (Run-of-Mine)	Pittsburgh #8 (DOE)	Pittsburgh #8 (SCS Cleaned)	Black Thunder
Quartz	22	9	6	27
Illite	22	9	10	2
Kaolinite	6	4	7	14
Pyrite	12	27	21	2
Calcite	2	3	0	<1
Mixed Carbonate	4	6	<1	<1
Misc. Silicates	23	19	18	24
Other	9	23	38	31
Area % <10μm	40	27	47	24

Table 3. Mössbauer Analysis of Coals (% of Fe in given phase)

Mössbauer File	Sample	Pyrite	Illite (Clay)	Siderite	Jarosite	Ferric Sulfate (?)
MK1695	Pittsburgh #8 (Kaiser)	75	11		14	
MK1698	Pittsburgh #8 (DOE)	90	8	3		
MK1697	Pittsburgh #8 (SCS)	34	7		22	37
MK1736	Pittsburgh #8 (SCS) [H_2O Washed]	59			41	
MK1699	Black Thunder	100*				

*Weak signal; CCSEM and chemical fractionation indicated approximately 50 to 60% iron as carbonate.

At each of the residence times considered, ash deposition tests, similar to those described elsewhere (Helble et al., 1992) were performed. The particle velocities at the point of impaction were kept constant at 1 and 5 m/s and gas temperature at the deposition probe surface was kept constant at approximately 1300°C. Ash samples were also collected using a nitrogen quenched probe and were subsequently analyzed for carbon content to determine the fractional burnout at the point (residence time) of deposition. Experiments are also being performed to collect ash samples under the same conditions for iron analysis by Mössbauer spectroscopy.

In Figure 1, data showing both the fraction of fixed carbon remaining and the ash collection efficiency are plotted as a function of time. The fixed carbon remaining was

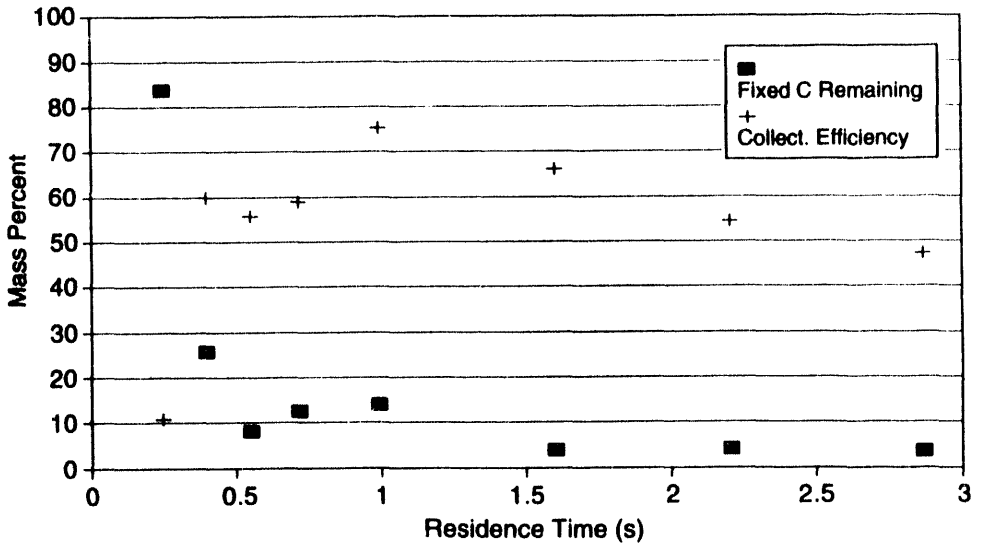

Figure 1. Burnout and stickiness comparison (washed Pittsburgh #8 (DOE)).

calculated using the proximate analysis for this coal and assuming that devolatilization was complete. This parameter was used to determine the fractional char burnout. From the plot we can see that the collection efficiency, (defined as the fraction of particles that traverse the tube flow cross-section, impact, and stick) increased between 0.25 and 0.40 seconds, with a maximum occurring at approximately 1 second. The collection efficiency continued to increase substantially after burnout was essentially complete (0.55 second). These data suggest that although high carbon contents (greater than 70%) in the ash may decrease ash stickiness, carbon plays at most a secondary role in ash stickiness. Pyrite oxidation, on the other hand, may cause the observed increase in stickiness due to the prolonged melt phase present during oxidation. The subsequent reduction of ash stickiness seen in Figure 1 may be caused by the oxidation of iron in glassy ash particles.

4. Effect of Iron Oxidation State on Ash Particle Stickiness

In order to better understand the effect of reducing conditions on ash deposition characteristics, a number of experiments are being conducted to measure the stickiness of glassy iron- containing ash particles as a function of iron oxidation state. Initial experiments were conducted in an atmosphere of 100% nitrogen at gas temperatures ranging from 900 to 1400°C. Ash particle collection efficiencies (on ceramic substrates that were assumed to be in thermal equilibrium with the surrounding gases) ranged from 50 to 60% at the highest temperature to 10 to 20% at the lowest temperature. Changing the gas composition to either 20% oxygen in nitrogen or 100% oxygen resulted in a significant decrease in collection efficiency at the highest temperatures. This is shown in Figure 2 for particles with an impaction velocity of 5 m/s; similar trends were observed for particles impacting the tube surfaces at 1 m/s. In either case, little difference between experiments conducted under 20% oxygen and those conducted under 100% oxygen was observed. From these initial experiments, it appears (1) that glassy ash particles containing iron in the (+2) oxidation state are stickier than those containing iron in the (+3) oxidation state and (2) that the oxidation of Fe^{+2} to Fe^{+3} in 20 to 80 μm ash particles occurs to the same extent in 20% and 100% oxygen at temperatures greater than 1000°C.

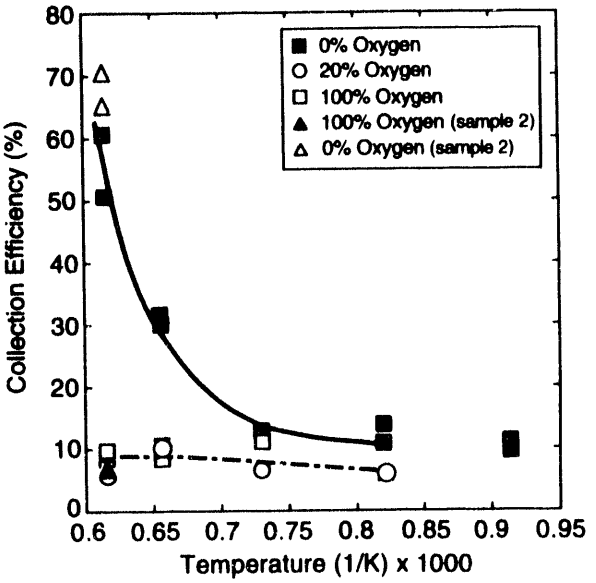

Figure 2. Collection efficiency for iron-containing glass particles as a function of temperature and oxygen partial pressure

5. In-Situ XAFS Measurements of Chemical Forms of Ash Compounds

PSI and U. Kentucky have developed and built a drop-tube furnace to be used for in-situ XAFS measurements of reacting coal and ash streams. It is designed to be separable into top and bottom sections so that it can be wheeled into the experimental hutch at the Brookhaven National Synchrotron Light Source and reassembled. The drop tube furnace is designed for one standard cubic foot per minute (scfm) total gas flow and one to 10 g/min of reactant feed rate. The input gas can be a mixture of two gases (nitrogen and oxygen) to produce varying oxidizing/reducing combustion conditions. About 80% of the total gas flow (primary air) is preheated to about 900 K before being injected to a diffuser, while the remaining 20% of gas flow is used to entrain the utility grind reactant (coal or mineral) from the auger feeder. The diffuser, at the top of the furnace, is designed to thoroughly mix the primary and feeder air and to distribute the solid particles uniformly across the entire flow cross sections in the alumina retort of the furnace. The 30-in. long, 3-in. i.d. alumina retort is electrically heated to achieve up to 1750 K wall temperature with a constant temperature zone of 20 in. At 1 scfm gas flow rate and 1500 K gas temperature the residence time of coal particles is about 1 s which is sufficient to achieve complete combustion of most coal particles. A conical ceramic venturi at the exit of the furnace reduces the outlet gas stream diameter from 3 to 1 in. diameter before it enters the X-ray section of the facility.

Figure 3 is a cut-away view of the analysis section which consists of a six-way cross designed to allow the X-ray beam and the detectors full access to the combustion product stream. Preliminary experiments using pyrite and Kentucky #9 coal were conducted during August 1993 with this facility. Additional tests are tentatively scheduled for March and July 1994.

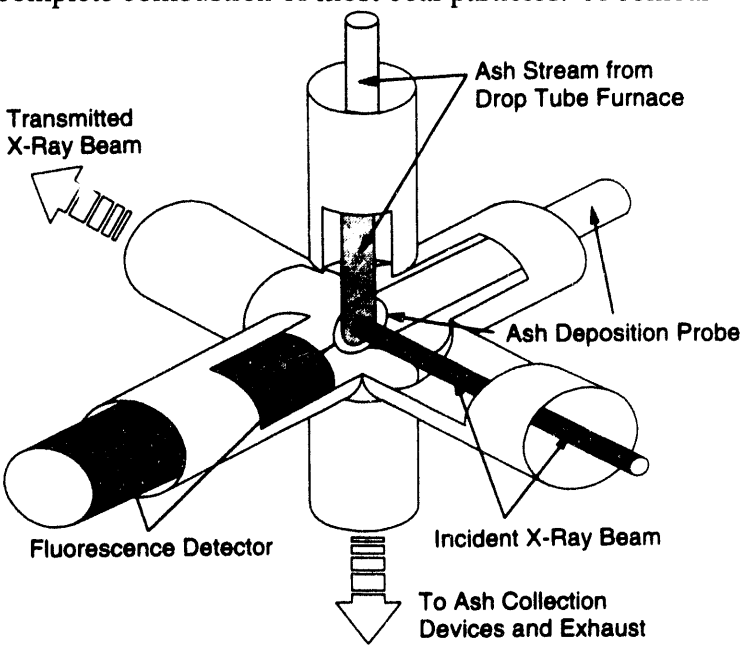

Figure 3. Cut-away view of six-way cross used for in-situ XAFS observation of ash stream and ash deposits

6. Engineering Model for Ash Formation - Developments

The Engineering Model for Ash Formation (EMAF) predicts the size and composition distributions of fly ash particles resulting from pulverized coal combustion. The input parameters for this model are divided into three categories: coal information, mineral information, and bulk ash information. Switches within the model permit char combustion, including the formation of char cenospheres (bituminous coals), and composition-dependent coalescence of individual mineral types to be considered. By affording fundamental control over the mechanisms of char combustion and mineral coalescence, the model can be used for a wide array of coal and mineral types. To date, it has been used with great success to predict ash size and composition distibutions. Recent efforts comparing model predictions with field data are described herein.

Two calculations were performed for a bituminous coal - one assuming cenosphere formation and one without. In the initial simulations (Figures 4), it was assumed that the coal did not swell during devolatilization. The mineral coalescence was divided into three different categories: "Full Coalescence" (all minerals coalesce), "Partial Coalescence" (selected minerals do not coalesce), and "1 Ash Per Mineral" (no minerals coalesce). The minerals not allowed to coalesce under the "Partial Coalescence" category, quartz and mixed carbonates, were selected based on the mineral composition and their known behavior in combustion systems. For example, pure quartz has a very high melting point and therefore would not likely form viscous melts to coalesce with other minerals. Illite, with a lower melting point, would be more likely to melt and coalesce. As seen in Figure 4, the EMAF predictions for "Partial Coalescence" agreed fairly well with the PSD for ash sampled from the first hopper of an ESP.

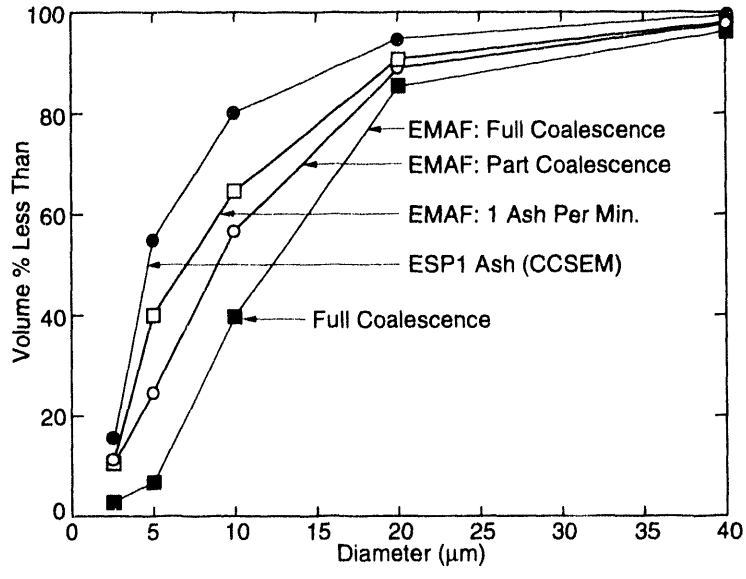

Figure 4. Ash PSD: model versus field data, no cenosphere formation

The second set of simulations were performed assuming the bituminous coal was a swelling coal. For this set of simulations, the coal was assumed to swell and form cenospheres during devolatilization. Only the "Full Coalescence" and "Partial Coalescence" categories described above were included. Results from the second set of simulations can be seen in Figure 5. The "Full Coalescence" case with cenosphere formation is very similar to the "Partial Coalescence" case without cenosphere formation. This suggests that not all of the minerals in

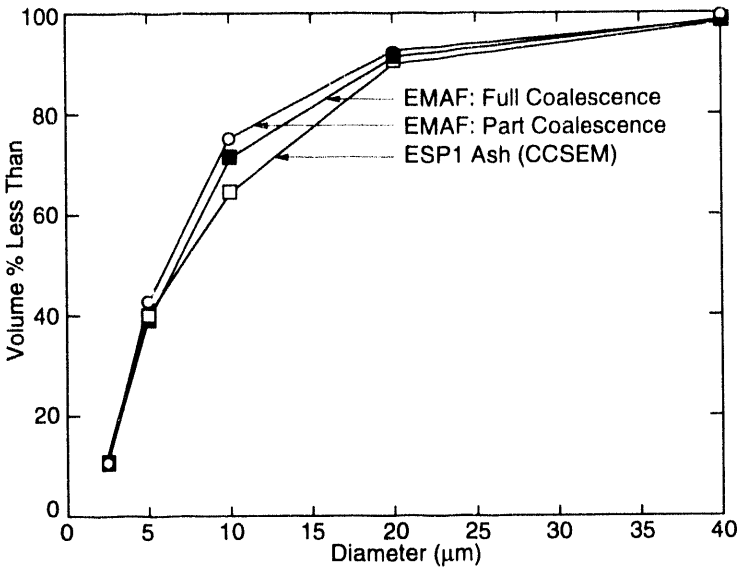

Figure 5. Ash PSD: model versus field data, cenosphere formation.

each coal particle coalesce - either due to cenosphere fragmentation, or limited melting of some minerals.

8. Future Efforts

During the year of this (two year) program, detailed experiments with the four program coals are planned. In addition to a continuation of the study of particle deposition described herein, experiments will address particle formation, including a study of the rate of iron oxidation and iron-aluminosilicate interactions. Using CCSEM and Mossbauer, analysis of the ash particle chemical composition distributions as a function of combustion stoichiometry will also be undertaken. Finally, additional in-situ XAFS measurements of iron and calcium behavior will be made in conjunction with the National synchrotron Light Source to assess for form of selected elements at elevated temperatures in flowing ash streams.

Acknowledgements

The authors wish to thank the VTT Technical Research Center of Fintad for providing the field CCSEM data for comparison with EMAF predictions.

References

Helble, J.J. et al. (1992), Transformations of Inorganic Coal Constituents in Combustion Systems, Final Report submitted to DOE/PETC under Contract DE-AC22-86PC90751.

DEPOSIT GROWTH AND PROPERTY DEVELOPMENT IN COAL-FIRED FURNACES

CONTRACT NUMBER: FWP Number: 0709

CONTRACTOR: Sandia National Laboratories
Combustion Research Facility
Livermore, California 94551-0969

PRINCIPAL INVESTIGATORS: Larry L. Baxter, (510) 294-2862
Donald R. Hardesty, (510) 294-2321

DOE PROJECT MANAGER: James D. Hickerson, PETC
Philip Goldberg, PETC

PROJECT OBJECTIVES AND DESCRIPTION

The objectives of this research project are (1) to provide a self-consistent database of simultaneously measured, time-resolved ash deposit properties in well-controlled and well-defined environments and (2) to provide analytical expressions that relate deposit composition and structure to deposit properties of immediate relevance to Combustion 2000 programs. This project is distinguished from other projects in the same research area by: (1) the development and deployment of *in situ*, diagnostics to monitor deposit properties, (2) the time resolution of such properties during deposit growth, (3) simultaneous measurement of structural and composition properties, (4) development of algorithms from a self-consistent database that includes the interdependence of properties, and (5) application of the results to technologically relevant environments such as those being planned under the Combustion 2000 program. The deposit properties of principal interest in this project include the heat transfer coefficient, porosity, emissivity, tenacity, strength, density, and viscosity.

This multi-year project began in October of 1993 and work on several of the subtasks is not scheduled to begin until later in the project. Recent results for those subtasks that are currently being pursued are discussed below. The six subtasks involved in this project include:

Subtask 2.1 Diagnostics for Coal Combustion Environments

Subtask 2.2 Experimental Determination of Transport, Thermal, and Structural Properties of Ash Deposits

Subtask 2.3 Analysis of Deposit Properties

Subtask 2.4 Chemical Reactions in Deposits

Subtask 2.5 Application to Combustion 2000 Program

Subtask 2.6 Documentation

BACKGROUND

Mineral matter in coal is cited as "the nemesis of coal-burning industries" and as playing "the dominant role in fuel selection, in setting the design and size of the furnace, and in establishing how that boiler furnace will be operated" [Raask, 1985]. However, the fate of mineral matter during pulverized coal combustion is relatively poorly understood, despite this importance to coal conversion systems. Significant progress in past years has been made through large measure because of PETC-sponsored research describing transformations of inorganic material during combustion. This new research project focuses on ash deposit formation and the development of deposit properties.

This research project supports the overall DOE mission of nurturing the effective and efficient use of national energy resources. It also supports the specific objective of the PETC mineral matter program to develop qualitative and quantitative understandings of mineral matter transformations in environments typical of pulverized-coal combustors and to incorporate these into tractable, mechanistic models. Major aspects of the project are designed to support DOE's Combustion 2000 program.

RECENT PROGRESS

This report focuses on one aspect of work performed under Subtask 2.1. A specific series of tests on two coals were conducted to demonstrate the use of advanced diagnostics to resolve deposition mechanisms chemical transformations on surfaces. The work being performed under this project enjoys the collaborative contirbutions from many people. All of the work reported here was performed at Sandia, much of it by Galen Richards as part of his doctoral research program at Brigham Young University. Galen's advisor is Dr. John Harb. Other significant collaborators include Everett Ramer (PETC), Peter Bernath (Univ. of Waterloo), Bryan Jenkins (UC Davis), Murray Abbott (CONSOL), Larry Dora (NIPSCO), and Terry Wall (Univ. of Newcastle).

Fuel Properties

The relevant properties of two coals for which specific results are illustrated in this paper are summarized in Table 1. They originate from reasonably close proximity in the Powder River Basin and have generally similar properties. The analyses indicated in the table are based on the supply used in the MFC during these tests. The average composition reported by the mines and by other researchers are even more similar to each other than these samples. Of particular importance in this study are the sulfur contents, silica to alumina ratio, sodium content, and calcium content. In all cases except calcium content, these properties are within expected sample-to-sample variation of one another when compared for the two coals. The calcium contents are also similar, although not within measurement uncertainty.

Despite these similarities, these two coals exhibit significantly different ash deposition behavior during combustion at both commercial and laboratory scales, even when tested in the same equipment under nominally identical combustion conditions. Traditional indices of ash behavior are based on algebraic combinations of elemental analyses. For two coals as similar as these, all of the traditional indices predict similar ash deposition behavior. The observations of significantly different behavior in the field and in laboratory tests indicates that the traditional indices, while valuable, are insufficient to capture the subtleties of ash deposition behavior.

Table 1

Proximate, ultimate, heating value, and ash analyses of the coals used in this investigation. Proximate and heating values are reported on a dry, ash-free basis.

	Antelope	Black Thunder	Ash Oxide	Antelope	Black Thunder
Moisture (%)	22.9	21.3	SiO_2	25.03	30.31
Ash (% dry)	5.51	6.46	Al_2O_3	11.36	16.27
Proximate (% daf)			Fe_2O_3	8.18	5.04
FC	54.2	42.0	TiO_2	0.66	1.27
VM	45.8	58.0	CaO	28.88	21.07
Ultimate (% daf)			MgO	5.60	4.74
C	72.4	74.8	Na_2O	1.57	1.41
H	5.2	5.4	K_2O	0.25	0.35
O	20.9	18.3	P_2O_5	0.81	0.91
N	1.1	1.0	SO_3	17.65	17.46
S	0.42	0.48	undeter.	0.01	1.17
Heating Value (daf - Btu/lb)	13562	13119			

Experimental Results

Experiments were conducted in Sandia's Multifuel Combustor (MFC), using an ash deposition probe and a Biorad FTS40/60 FTIR spectrometer. This equipment and its use is described elsewhere [Baxter, 1993; Baxter, et al., 1993].

Figure 1 illustrates recently analyzed [Baxter, et al., 1993; Richards, et al., 1994 (in press); Richards, et al., 1994] FTIR spectra during ash deposition on the probe in the MFC. A series of three spectra are indicated, with the initial spectrum offset by a value of 0.4 along the ordiante so that it is conveniently displayed witht he subsequent two spectra. In addition to the initial spectrum, on spectrum collected 10 minutes into the ash deposition process is indicated, with a second spectrum collected at 30 minutes.

In these spectra, the development of prominent features in 1075-1175 cm^{-1} region is prominent. This region of the spectrum includes contributions from silica, silicates, and sulfates. The S-O stretch of the sulfate cation contributes to the signal predominantly at the high wavenumbers. (Similar silica vibrations contribute around 1100 cm^{-1}.) There is some influence of the anion in the suflate salt on the frequency of this vibration. This shift in vibration frequency (or energy) offers the potential to determine which sulfate species are predominantly contributing to the spectrum. In our past reports we have illustrated cases where the features associated with different sulfates are clearly separated. In the spectrum below, the features overlap significantly and assignment of specific sulfate species to the features is more difficult. Qualitatively, we expect the spectral features to shift to higher wavenumbers as the sulfates change composition from sodium-based to calcium based. The shift is expected to be of order 10-15 cm^{-1}. The spectra shown in Fig. 1 are consistent with this interpretation.

The features at lower wavenumbers are associated with alumino-silicates. These, too, are

influenced by anions such as sodium, potassium, and calcium, that are bound to the SiO_x backbone. Many alkali-aluminosilicates have features in the region between 1050 and 900 cm^{-1}.

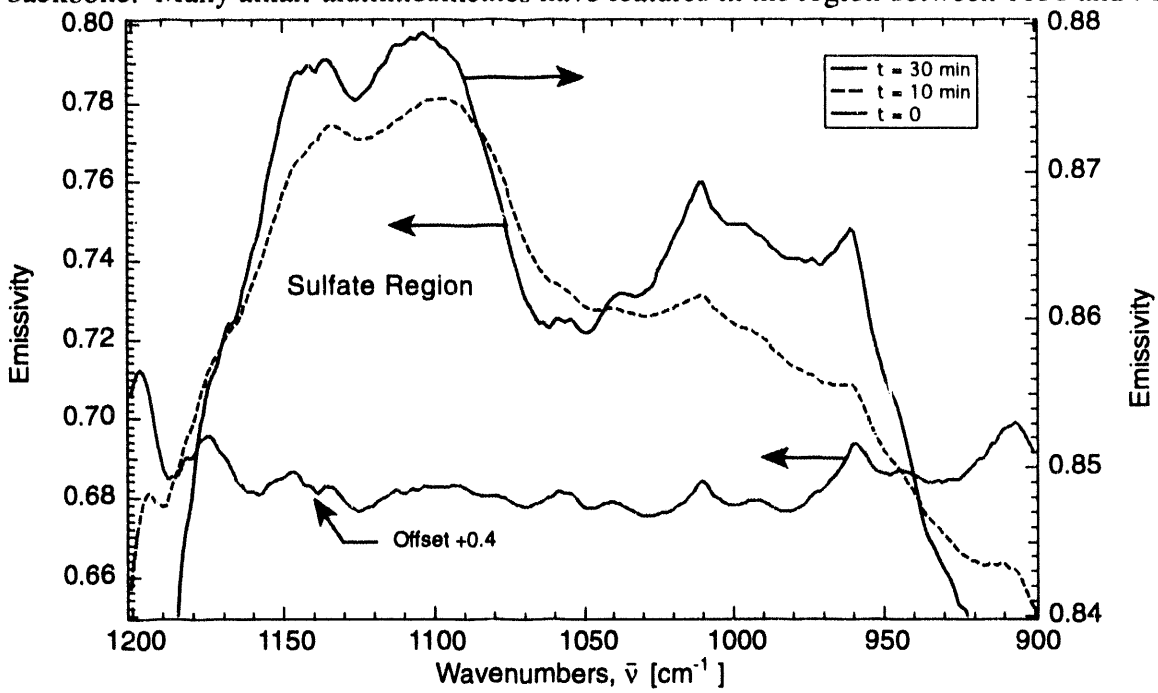

Figure 1 Spectral emissivity of deposits formed from the Black Thunder coal as a function of time during the early stages of deposition. Spectra indicate substantial increase in silica and sodium-based sulfates (note that initial spectrum is offset by 0.4) during the first 10 minutes of deposition. The more subtle shift in prominent spectral features to higher wave numbers with increasing deposit accumulation time is indicative of transformation of sodium-based sulfates to calcium-based sulfates. Similar spectra were observed for the Antelope coal.

Figure 2 illustrate similar data over a broader wavelength region and over longer deposition time for these two coals. The essential features of the data that are germane to this discussion are that while both deposits contain significant sulfate and silicate material, the Antelope coal shows greater evidence of sulfate formation, whereas the Black Thunder coal shows greater evidence of aluminosilicate formation.

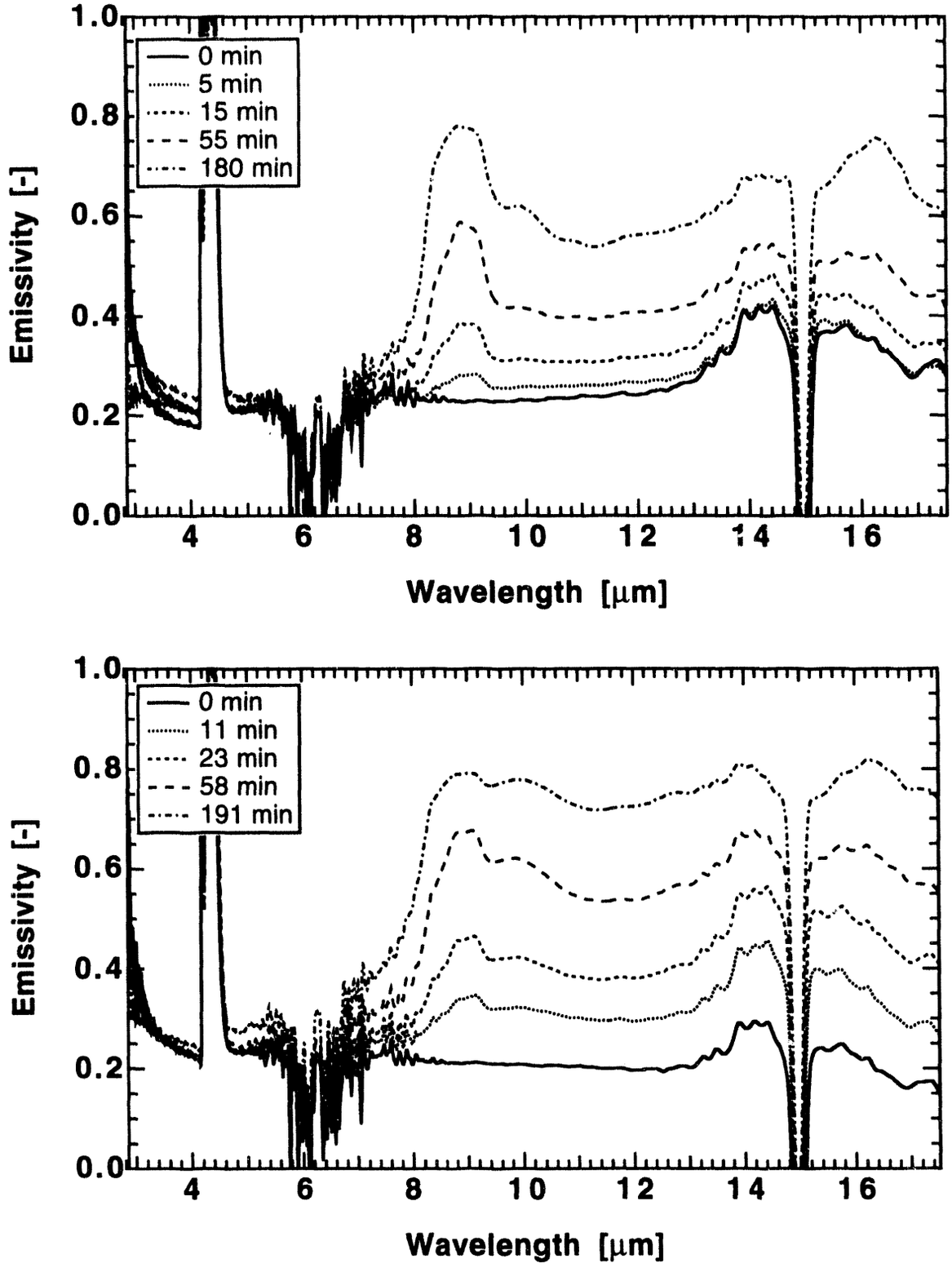

Figure 2 Spectral emissivity measurements for ash deposits generated from the Antelope coal (top) and the Black Thunder coal (bottom) during the first 3 hours of deposition.

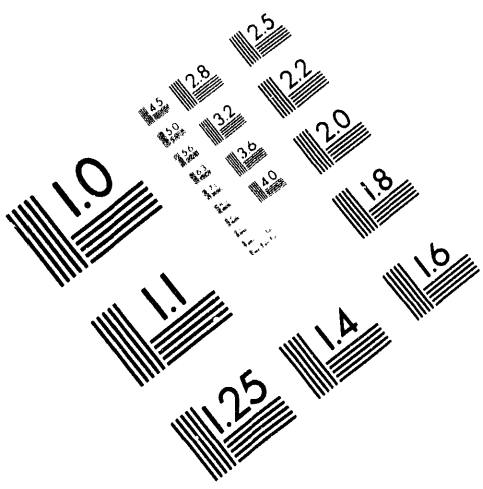

Association for Information and Image Management
1100 Wayne Avenue, Suite 1100
Silver Spring, Maryland 20910
301/587-8202

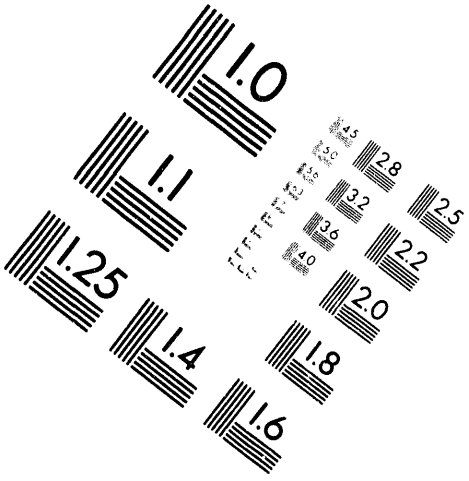

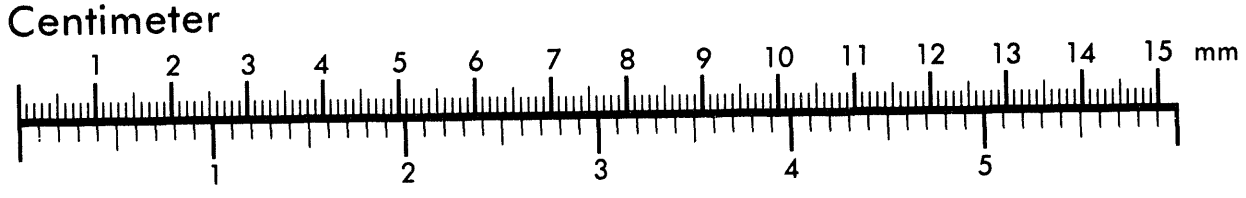

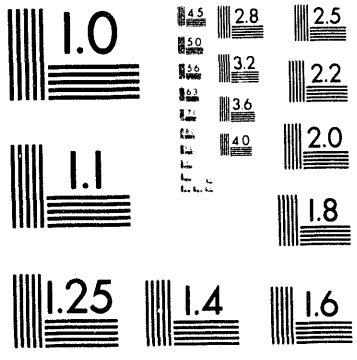

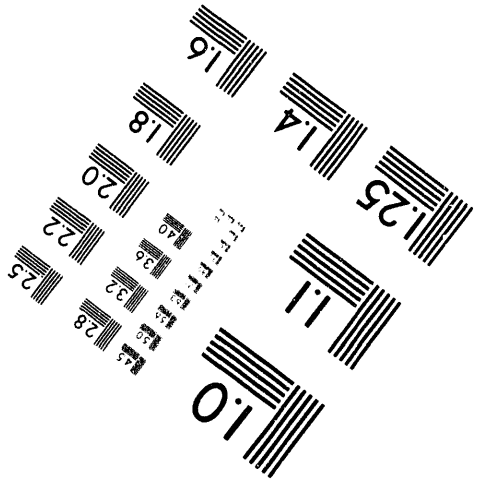

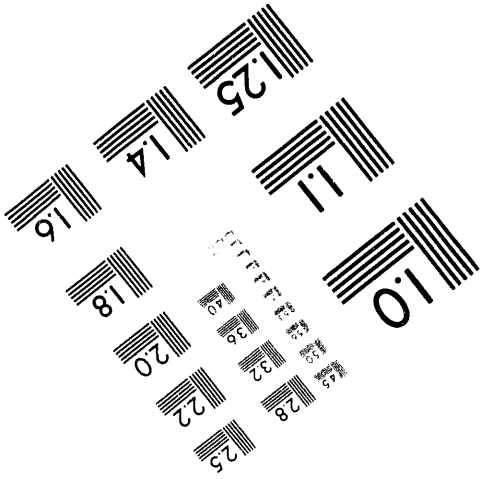

MANUFACTURED TO AIIM STANDARDS
BY APPLIED IMAGE, INC.

2 of 4

The substantially larger concentrations of sulfates in the Antelope deposits as compared to the Black Thunder deposit has been verified several ways. Table 1 indicates the elemental composition of the deposits formed from both coals, together with the composition of the ash generated from the fuel. The substantial differences in composition indicated by the FTIR emission spectroscopy are also evident in the overall composition (note sulfur silica/alumina in deposits, for example). More detailed analyses using SEM images [Richards, et al., 1994 (in press)] confirms the presence of calcium and alkali sufates on surfaces of the probes and particles. The extent of sulfation is much higher for the Antelope coal than for Black Thunder (especially on the probe surface).

Table 2

Ash elemental analyses for the coals and deposits discussed in this investigation, expressed as percent of total ash.

	Coal Ash		Deposit	
Ash Oxide	Antelope	Black Thunder	Antelope	Black Thunder
SiO_2	25.03	30.31	28.51	43.83
Al_2O_3	11.36	16.27	11.45	16.51
TiO_2	0.66	1.27	0.75	1.59
Fe_2O_3	8.18	5.04	10.23	6.05
CaO	28.88	21.07	33.1	23.5
MgO	5.6	4.74	6.18	4.92
K_2O	0.25	0.35	0.31	0.21
Na_2O	1.57	1.41	1.3	0.39
SO_3	17.65	17.46	5.17	1.71
P_2O_5	0.81	0.91	1.64	1.16
undetermined	0.01	1.17	1.36	0.13

Conclusions

FTIR emission spectroscopy was applied to deposits generated from similar coals to determine the composition and mechanisms of ash deposition. Two coals that are similar in elemental composition, but different in their ash deposition characteristics when tested at commercial scale, were used in these tests. The two coals were determined to form deposits that differed in the relative sulfate and silicate compositions. Sulfates were shown to shift from sodium-based compounds to calcium-based compounds as ash deposits grow in both coals. Sodium-based sulfates form through condensation mechanisms on the surface of the probe, followed by sulfation with gas-phase sulfur. Calcium-based deposits form by sulfation of calcium oxide particles after their deposition, by impaction, on the probe surface.

The differences in deposit chemistry and the mechanisms of deposit formation are supported by SEM images of the deposits and by elemental analyses of the ash. SEM images show that

sodium sulfates are concentrated on the probe surface, whereas calcium sulfates form on the surface of calcium-oxide particles. Elemental analysis of the deposits of the two coals supports the significantly different amount of sulfation in the two coals, with one deposit showing sulfur concentrations that exceed that of the other coal by a factor of 3.

These data provide definitive indications of the differences in the deposit chemistry and growth mechanisms. Pilot-scale facilities were able to successfully create conditions sufficiently similar to full-scale operation that the differences in deposit morphology, chemistry, and growth mechanisms could be studied. As a whole, this study illustrates the necessity for comlementary information to the ASTM analyses to understand ash deposit formation in coal combustors.

FUTURE PLANS

Further development and validation of the FTIR emission diagnostic will be completed this year. Also, development of *in situ* diagnostics for determining the concentration of inorganic vapors in combustion environments will be initiated. Summary reports on release mechanisms and fragmentation will be produced this fiscal year. In future years, fundamental relationships between deposit morphology, chemistry and transport properties will be pursued both theoretically and experimentally.

ACKNOWLEDGMENTS

Many of the chemical and physical analyses of solid samples of fly ash, deposits, and raw coal gathered during this work are performed by CONSOL Inc. Galen Richards (Graduate Student, BYU) performed many of the FTIR measurements in the combustor. Gian Sclippa (TAD Technician) and Al Salmi (Sandian) are also instrumental in operating and maintaining the combustor and in design and construction of diagnostic and probe equipment.

REFERENCES

The following references include papers cited above and other published papers resulting from PETC-supported work related to this project that appeared in the last twelve months.

Baxter, L. L. (1993). "In Situ, Real-Time Emission FTIR Spectroscopy as a Diagnostic for Ash Deposition During Coal Combustion". In *Engineering Foundation Conference on The Impact of Ash Deposition on Coal-Fired Plants*, . Solihull, England:

Baxter, L. L., Richards, G. H., Ottesen, D. K., and Harb, J. N. (1993). "*In Situ*, Real-time Characterization of Coal Ash Deposits Using Fourier Transform Infrared Emission Spectroscopy." ***Energy & Fuels***, *7*(6), 755-760.

Raask, E. (1985). *Mineral Impurities in Coal Combustion.* Washington: Hemisphere Publishing Corporation.

Richards, G. H., Harb, J. N., and Baxter, L. L. (1994 (in press)). "Investigation of Mechanisms for the Formation of Fly Ash Deposits from Two Low-Sulfur Western Coals." ***Energy & Fuels***.

Richards, G. H., Harb, J. N., Baxter, L. L., Bhattacharya, S., Bupta, R. P., and Wall, T. F. (1994). "Radiative Heat Transfer in PC-Fired Boilers — Development of the Absorptive/Reflective Character of Initial Ash Deposits on Walls". In *Twenty-Fifth Symposium (International) on Combustion*, . Irvine, CA: The Combustion Institute.

PRESENTATIONS AND PUBLICATIONS

The following publications were sumbitted in the last year based in part or in whole on PETC-sponsored work.

Baxter, L. L. (1993a). "Ash Deposition During Biomass and Coal Combustion: A Mechanistic Approach." ***Biomass and Bioenergy***, ***4***(2), 85-102.

Baxter, L. L. (1993b). "In Situ, Real-Time Emission FTIR Spectroscopy as a Diagnostic for Ash Deposition During Coal Combustion". In *Engineering Foundation Conference on The Impact of Ash Deposition on Coal-Fired Plants*, . Solihull, England:

Baxter, L. L. (1994 (in press)). "Development of Emission FTIR Spectroscopy as a Diagnostic for Ash Deposition During Coal Combustion." ***Combustion and Flame***.

Baxter, L. L. (1994 (to appear)). "In Situ, Real-Time Analysis of Ash Deposit Chemistry During Pulverized Coal Combustion." ***Energy & Fuels***.

Baxter, L. L., and DeSollar, R. W. (1993). "A Mechanistic Description of Ash Deposition During Pulverized Coal Combustion: Predictions Compared to Observations." ***Fuel***, ***72***(10), 1411-1418.

Baxter, L. L., Miles, T. R., Miles, T. R., Jr., Jenkins, B. M., Richards, G. R., and Oden, L. L. (1993a). "Transformations and Deposition of Inorganic Material in Biomass Boilers". In M. G. Carvalho (Ed.), *Second International Conference on Combustion Technologies for a Clean Environment*, 1 (pp. Biomass II: 9-15). Lisbon, Portugal: Commission of European Communities.

Baxter, L. L., Mitchell, R. E., and Fletcher, T. H. (1994 (to appear)). "Release of Inorganic Material During Coal Devolatilization." ***Combustion and Flame, to appear***.

Baxter, L. L., Richards, G. H., Ottesen, D. K., and Harb, J. N. (1993b). "*In Situ*, Real-time Characterization of Coal Ash Deposits Using Fourier Transform Infrared Emission Spectroscopy." ***Energy & Fuels***, *7*(6), 755-760.

Baxter, L. L., and Smith, P. J. (1993). "Turbulent Dispersion of Particles: The STP Model." ***Energy & Fuels***, *7*(6), 852-859.

Richards, G. H., Harb, J. N., and Baxter, L. L. (1994 (in press)). "Investigation of Mechanisms for the Formation of Fly Ash Deposits from Two Low-Sulfur Western Coals." ***Energy & Fuels***.

Richards, G. H., Harb, J. N., Baxter, L. L., Bhattacharya, S., Bupta, R. P., and Wall, T. F. (1994). "Radiative Heat Transfer in PC-Fired Boilers — Development of the Absorptive/Reflective Character of Initial Ash Deposits on Walls". In *Twenty-Fifth Symposium (International) on Combustion*, . Irvine, CA: The Combustion Institute.

Wall, T. F., and Baxter, L. L. (1993). "Ash Deposits, Coal Blends, and the Thermal Performance of Furnaces". In *Engineering Foundation Conference on Coal Blending and Switching of Western Low-Sulfur Coals*, . Snowbird, Utah:

The following manuscript was unavailable at the time of publication.

FUELS EVALUATION FACILITY-USE OF VITIATED AIR IN COMBUSTION

S. Smouse
Pittsburgh Energy Technology Center
P.O. Box 10940
MS 84-340
Pittsburgh, PA. 15236

Please contact author(s) for a copy of this paper.

THE PHYSICS OF NON-NEWTONIAN LIQUID SLURRY ATOMIZATION PART2: TWIN-FLUID ATOMIZATION OF NON-NEWTONIAN LIQUIDS

ADEL MANSOUR AND NORMAN CHIGIER
DEPT OF MECHANICAL ENG. CARNEGIE MELLON UNIV.
PITTSBURGH, PA. 15213

ABSTRACT

The changes in the physical processes of atomization as a result of adding a high molecular weight polymer in low concentrations to liquid have been studied. Both Newtonian and non-Newtonian liquids were investigated with particular emphasis on the non-Newtonian rheological characteristics. It was found that viscoelastic liquids are much more difficult to atomize than viscoinelastic liquids. Viscoinelastic liquids showed a breakup behavior similar to that of water sprays. Viscoelastic materials showed remarkably different breakup patterns. The ligaments were seen to undergo a very large stretching motion before they breakup, resulting in long threads of liquid attached to droplets. The normal stresses developed in viscoelastic materials are much higher than their associated shear stresses. Consequently, the development of the large normal stresses appears to be the most important rheological mechanism that inhibits breakup.

INTRODUCTION

Airblast atomization of viscous non-Newtonian liquids is carried out using a co-axial twin-fluid atomizer [1]. As the atomizing air interacts with the liquid jet downstream form the nozzle exit, waves form on the surface of the liquid jet. As a result, the liquid jet sheds ligaments which rapidly collapse into droplets. The atomized drop sizes can be described in terms of three dimensionless groups, namely the liquid/air mass ratio (M_l/M_a), Weber ($We = \rho_g D U_g^2/\sigma$) and Ohnesorge ($Z = \mu_l/(\rho_l \sigma D)^{1/2}$) numbers in simple forms whose exponents and coefficients are determined by least squares fit to the experimental data. A phase Doppler particle analyzer was used for the determination of particle size and velocity. A digital spray analyzer was used for die-swell measurements. The Non-Newtonian liquids selected for the experiment were aqueous solutions of Xanthan gum (supplied by Aldrich Chemical Co.) and Polyacrilamide E10 (supplied by Allied Colloid Co.). Tests were performed on 0.05, 0.10, 0.15, 0.20, 0.30% concentrations by mass for the Xanthan Gum polymer, and 0.0125, 0.025, 0.05, 0.1, 0.15, 0.30, and 0.50% concentrations by mass for the Polyacrilamide E10.

RHEOLOGICAL MEASUREMENTS

Shear Viscosity Measurements The rheology of the polymeric solutions was modeled by the Power Law Model.

$$\tau = k\,|\dot{\gamma}|^{n-1}\,\dot{\gamma} \qquad (1)$$

where τ is the shear stress, $\dot{\gamma}$ is the shear rate, n is the power law index and k is the consistency index. Viscosity measurements at low shear rates ($\dot{\gamma} < 13.4\ s^{-1}$) were performed using the Brookfield viscometer. To obtain viscosity data at higher shear rates ($\dot{\gamma} > 13.4\ s^{-1}$), capillary tube viscometers were used. A large and small capillary tube were operated in the range of shear rates, $10 < 8V/D < 2000\ s^{-1}$ and $1800 < 8V/D < 20000\ s^{-1}$, respectively. In order to eliminate the errors associated with the velocity adjustment region in the entrance and exit of the capillaries a differential pressure measurement system was utilized. A highly accurate differential pressure transmitter was used to obtain the pressure drop across two points on each capillary tube. The large and small tube diameters were 4.39 mm and 1.80 mm, with a length to diameter ratio of 80 and 189, respectively.

The apparent viscosity data for the Xanthan and E10 solutions is shown in Figs 1 and 2, respectively. In the mid-range of shear rates ($10 < \dot{\gamma} < 3500\ s^{-1}$), the apparent viscosity conforms to a power-law function. In the highest range of shear rates, $\dot{\gamma} > 3500\ s^{-1}$, the apparent viscosity becomes nearly constant and the solutions tend towards Newtonian behavior, with viscosities relatively close to that of water. The degree of shear thinning exhibited by each solution was characterized by the apparent viscosity power law index in the mid-range of shear rates. For each concentration, the power law

parameters and apparent viscosity limiting values are summarized in Table 1. η_o is the viscosity value that is reached in the limit as the shear rate tends towards zero. The value η_∞ is the apparent viscosity value which is reached as the fluid becomes Newtonian at high shear rates. It is observed from Table 1 that n is a strong function of the solution concentration with a decreasing value of n for increasing values of concentration.

Table 1: Power-Law Parameters and Limiting Viscosities for Xanthan and E10 soluions

Conc. (%)	k (cP-S^{n-1})	n	η_o (cP)	η_∞ (cP)
0.05XG	28.6	0.604	30	1.6
0.10XG	110.2	0.487	115	1.7
0.15XG	321.0	0.383	822	1.8
0.20XG	664.4	0.333	2416	2.2
0.30XG	1804.8	0.248	14761	2.8
0.0125E10	1.9	0.923	2.10	1.2
0.025E10	3.2	0.855	3.40	1.3
0.05E10	7.3	0.757	7.912	1.5
0.10E10	18.7	0.700	20.21	2.2
0.15E10	84.4	0.595	93.00	3.9
0.30E10	517.7	0.444	1243	6.3
0.50E10	1644.4	0.387	9342	12.1

Die-Swell Measurements The phenomenon of die-swell is attributed to the relaxation of the normal stresses. In order to calculate the normal stresses from die-swell, the following relationship proposed by Metzner and co-workers [2] is used.

$$N_1 = \tau_{11}-\tau_{22} = \frac{\rho D^2(8V/D)^2}{64\ n'}\left\{(n'+1)\left(\frac{3n+1}{2n+1}\right) - \left(\frac{D}{d_j}\right)^2\left[n'+1+\frac{d\ log\ D/d_j}{dlog\ 8V/D}\right]\right\} \qquad (2)$$

Measurements of the die-swell ratio (D/d_j) along with the volumetric flow rate are used to evaluate the normal stress differences. A digital image analyzer with a close-up lens was positioned near the outlet of the capillary tube to measure the jet diameter. The jet diameter and volumetric flow rate were measured at different flow conditions. Figure 3a and 3b show a typical image of the die-swell phenomenon for 0.3% Xanthan and 0.5% E10 solutions respectively at a shear rate 8V/D = 5246 S^{-1}. In order to calculate the normal stress difference from die-swell measurements, a reasonably accurate estimate of the shear dependency as a function of 8V/D is needed. Over the range of 8V/D for which die-swell measurements were made (300 sec^{-1} < 8V/D < 5000 sec^{-1}), the shear dependency of the polymeric solutions is represented by the values of n shown in Table 1. The calculated values of the first normal stress differnce N_1 as a function of shear rate for the Xanthan and E10 solutions are given in Fig.4. The single most important difference between the Xanthan solutions and the E10 solutions is the much higher levels of normal stresses developed in the E10 solutions when compared to the Xanthan gum solutions.

AIRBLAST ATOMIZATION

Dependence of SMD on Fluid Viscosity or the Ohnesorge number. Local point measurements of the Sauter mean diameter were made at r = 0 and x/D_a = 20, where x is the downstream distance from the injector, r is the radial distance, and D_a is the annular air jet diameter. The variation of the Sauter mean diameter of droplets with changes in the air/liquid ratio is shown in Fig. 5. Throughout this experiment the air flow rate was maintained constant at 12.89 g/s and the liquid flow rate was varied between 2.27g/s and 27.21 g/s. This corresponds to an air velocity of 93.4 m/s and a liquid velocity varying from 0.310 to 3.72 m/s. Atomization data for the highest concentrations of Polyacrilamide E10 solutions (i.e., 0.05, 0.1, 0.15, 0.3, 0.5) are not included in Fig. 5. For these concentrations the liquid did not atomize. Long threads of liquid interspaced by droplets were formed and the rejection rate due to phase errors exceeded 30% for the highest concentration.

Figure 5 shows that, although the shear viscosity data for the 0.025% solution of E10 is orders of magnitude lower than that of the 0.3% solution of Xanthan at all values of the shear rate,

the atomization quality of the Xanthan solution is substantially better at all values of the liquid flow rate. The single most important difference between the Xanthan solution and the E10 solution is the much higher levels of normal stresses developed in the E10 solution. The large die-swell ratio (dj/D) that has been observed for the E10 solutions in the capillary tube experiment suggests that the extensional viscosity levels for the E10 solutions are large and that the extensional viscosity is probably the most important rheological mechanism that inhibits breakup. Figure 5 also shows the significant reduction in droplet size that can be obtained by increasing the air/liquid mass ratio.

The effects of solution rheology on atomization are first examined in order to determine which viscosity should be used to define the Ohnesorge number. The spray mean drop size data shows that the SMD increases with apparent viscosity of the fluid. The liquid flow rate was varied between 2.27 g/s and 27.21 g/s corresponding to an apparent shear rate (8V/D) inside the injection tube varying between 786 S^{-1} and 9754 S^{-1}. Due to the very high shear rates encountered inside the atomizer, it was decided to correlate the data in terms of η_∞. The reason for maintaining the air flow rate constant was to remove any extraneous effects of the additional shear introduced by the air flow on the fluid viscosity. The data in Fig. 5 was fitted to the following equation:

$$SMD \ \alpha \ Z^{X_Z} \qquad (3)$$

Only water and the 0.05, 0.1, 0.15, 0.2 and 0.3% solution of Xanthan are considered for the correlation. The data consisted of 19 data sets representing the various variations of liquid flow rate, and each data set contained 6 points representing the various polymer concentrations. Each of the data sets was fitted to Eq. (3) separately to show the functional dependence of the SMD on fluid viscosity. The power-dependency X_Z of the Sauter mean diameter on fluid viscosity, in the limit of infinite shear rates, is shown in Fig. 6. In Fig. 6 X_Z is plotted as a function of the apparent shear rate (8V/D) inside the injection tube. It is seen in Fig. 6 that the exponent X_Z is not constant and is a function of the shear rate. At the low end of shear rates ($8V/D < 3600\ S^{-1}$), the exponent X_Z decreases with shear rate. Beyond $8V/D = 3600\ S^{-1}$, X_Z remains sensibly constant. The variations of X_Z with respect to the shear rate is relatively simple to explain in terms of the apparent viscosity of the fluid. At the low end of shear rates, the liquid inside the injection tube is sheared to a consistency which intermediate between η_0 and η_∞. The use of η_∞ to correlate the SMD data with is not appropriate. At shear rates above 3600 S^{-1}, the liquid inside the atomizer is sheared to a consistency η_∞ for all concentrations and the use of η_∞ to correlate the SMD data with is indeed the most appropriate choice. The average value of X_Z at shear rates greater than 3600 S^{-1} is $X_{Z,av} = 0.417$. Attempts at correlating the data in terms of a mass averaged shear viscosity, which is seemingly a more appropriate choice, were unsuccessful. The reason for this is that correlation of the data in terms of a mass averaged shear viscosity requires knowledge of the velocity profile at the exit of the injection tube, which is not known apriori. Even if the velocity profile were known, correlating the data based on a mass averaged shear viscosity would make the problem untractable since the mass average shear viscosity is not single valued; it varies with shear rate. Figure 6 shows that SMD increases in proportion to the increase of the apparent viscosity. Note that the correlation is valid for viscoinelastic liquids only (Xanthan solutions). The coefficient of dependence in the high shear rate region ($X_Z = 0.417$) is not far removed from previous results with Newtonian liquids.

The air flow field in airblast atomization is unknown. The air flow imparts additional shear on the liquid column before breakup. Although, at low liquid flow rates, the liquid inside the injector might not have been sheared to a consistency η_∞, the additional shearing imparted to the liquid due to its interaction with the air flow can result in additional thinning of the liquid before breakup. Thus, a second set of experiments were carried out to investigate if the additional shear, on the liquid column before breakup, introduced by the air flow has any effect on the power dependency (X_Z). The liquid velocity was maintained constant at $M_l = 7.46$ g/s, corresponding to $8V/D = 2622S^{-1}$ and the air mass flow rate was varied between 8.51 g/s and 23.64 g/s corresponding to an air velocity in the range of $61.66\ m/s < V_a < 171.278\ m/s$. This resulted in Weber number variation between 189 and 1461. This experiment was carried out using pure water

and the 5 Xanthan solutions. The data consisted of 17 data sets representing the various variations of air flow rate, and each data set contained 6 points representing the various polymer concentrations. Figure 7 shows that the SMD decreases with increase in the Weber number. Each of the data sets was fitted to Eq. (3) separately to show the functional dependence of the SMD on fluid viscosity at variable air flow or Weber number. Figure 8 shows that X_z is insensitive to the variations in air mass flow rate or air velocity. It was found that the power dependency X_z remains almost the same with $X_{z,av} = 0.420$.

Dependence of SMD on $1+M_l/M_a$ The power-dependence on $(1 + M_l/M_a)$ is examined by plotting the SMD data as a function of $(1 + M_l/M_a)$ at constant Weber number. Figure 9 shows the same data displayed in Fig. 5 as a function of $(1 + M_l/M_a)$ plotted using a logarithmic plot. It should be noted that the slope of the line shown in Fig. 9 is effectively unity. Therefore the power of $(1+M_l/M_a)$ in the SMD equation, should be unity.

Dependence of SMD on Weber Number Experiments were conducted to examine the influence of Weber number on the Sauter mean diameter. The effect of Weber number on droplet SMD was examined by varying the air exit velocity. No variations of surface tension were undertaken. The data presented in Fig. 7 was used to establish the functional dependence of the SMD on the Weber number. The power-dependence on Weber number is examined by plotting the SMD data as a function of Weber number at constant $(1 + M_l/M_a)$. In the previous sections we have established that the effects of the air flow on the viscous behavior of the polymeric solutions are negligible. Recall that the power dependency X_z of the SMD on η_∞ was nearly constant, irrespective of the Weber number, with $X_{z,ave} = 0.420$. In the previous section we have also established that the power-dependency of SMD on $(1 + M_l/M_a)$ is unity. Thus, in order to extract the Weber number dependency from the data presented in Fig.7, the SMD should be divided by $(1 + M_l/M_a)$. The data of Fig.7 was thus correlated by the following Equation:

$$SMD/(1 + \dot{M}_l/\dot{M}_a) \propto We^{-X_w} \qquad (4)$$

Table 2 shows the best least squares solutions of the unknown variables X_w for water and the 5 Xanthan solutions. The correlation coefficients are found to be in the range 0.977 to 0.992. The average value of Weber number dependency X_w is $X_{w,av} = 0.503$.

Table 2 Weber Number Dependency

Solution	X_w	c.o.c
Water	0.507	0.992
0.05% XG	0.482	0.977
0.10% XG	0.518	0.981
0.15% XG	0.504	0.986
0.20% XG	0.505	0.980
0.30% XG	0.502	0.990

General Semi-Empirical Model for Airblast Atomization The wave mechanism has found the most wide acceptance among the mechanisms of atomization. Atomization is a process whereby a volume of liquid is converted into waves, ligaments and drops. When the dynamic pressure $(\rho_a U_a^2/2)$ of the air stream in airblast atomization is large enough, the amplitude of the surface waves will grow if their wavelength (λ) exceeds a minimum value ([3]; [4]). When the amplitude becomes sufficiently large, the waves shed ligaments which rapidly collapse, forming drops. When the aerodynamic pressure force predominates, waves propagate as acceleration waves and are governed by $(Z/We)^{2/3}$. In contrast, when the surface tension predominates, waves propagate as capillary waves and are governed by (Z^2/We) [3, 5]. Therefore, both We and Z, with exponents of the Z number equal to or twice that of the We-dependency, are included in our modeling of drop sizes for airblast atomization.

Based on the aforementioned wave mechanism, the following two and three-parameter models are proposed along with the basic drop size equation for air blast atomizer, Eq. (5), [6]. Equations (5), (6a), (6b), (6c), and (6d) are used to correlate the data in terms of the Weber

number, the Ohnesorge number, and the non-dimensional group $(1+M_l/M_a)$. The linear dependence on $(1+ M_l/M_a)$ is based on momentum balance and energy considerations [5]. The power dependency of unity was verified in a previous section.

$$SMD/D = (1 + \dot{M}_l/\dot{M}_a)\left[X_2\ We^{-0.5} + X_3\ Z^{1.0}\right] \quad (5)$$

$$SMD/D = (1 + \dot{M}_l/\dot{M}_a)\left[X_2 We^{-X_1} + X_3\ Z^{X_1}\right] \quad (6a)$$

$$SMD/D = (1 + \dot{M}_l/\dot{M}_a)\left[X_2 We^{-X_1} + X_3\ Z^{2X_1}\right] \quad (6b)$$

$$SMD/D = (1 + \dot{M}_l/\dot{M}_a)\left[X_2\ (Z/We)^{X_1}\ \right] \quad (6c)$$

$$SMD/D = (1 + \dot{M}_l/\dot{M}_a)\left[X_2\ (Z^2/We)^{X_1}\ \right] \quad (6d)$$

The exponents and coefficients are determined by least squares fit of these equations to more than 220 experimental points.Table 3 shows the best least squares solutions of the three unknown variables X_1, X_2, and X_3 of Eqs. (5), (6a), (6b), (6c), and (6d) along with the coefficients of correlation. The coefficients of correlation were found to be in the range 0.933 to 0.972. The best correlations are found for the equations involving the exponent of the Z-dependency equal to the exponent of the We-dependency. This verifies the basic intuition that at the conditions of the study the waves propagate as acceleration waves. The correlation coefficient of Eq. (6c) is particularly good especially that the equation involves only two parameters (X_1 and X_2). Figure 10 demonstrates the agreement between the proposed models with the best least squares solutions listed in Table 3 and the experimental data. The agreement is considered excellent in view of the diverse liquid properties and experimental conditions.

Table 3 Semi-Empirical Model for Airblast Atomization of Non-Newtonian Viscoinelastic Fluids

	X_1	X_2	X_3	c.o.c
Eq. (3)	—	0.169	0.581	0.964
Eq. (6a)	0.616	0.264	0.125	0.972
Eq. (6b)	0.390	0.0707	0.275	0.969
Eq. (6c)	0.496	3.414	—	0.969
Eq. (6d)	0.328	2.930	—	0.933

Acknowledgements The authors gratefully acknowledge financial support from DOE, PETC, grant number DE-FG22-92PC92152.

References

1. Mansour A., " The Effects of Non-Newtonian Rheology and Liquid Turbulence on Twin Fluid Atomization" PhD Thesis, Dept. of Mech. Eng. Carnegie Mellon Univ. Pgh, PA (1994).
2. Metzner, A.B., Houghton, W.T., Sailor, R.A., and White, J.L., Trans. Soc. Rheo, V, 133, 1961.
3. Jeffreys, H., Roy. Soc. Proc., Series A, Vol. 107, pp. 189-206, (1925).
4. Adelberg, M., AIAA J., Vol.5, pp1408-1415, (1967).
5. Tsai, S.C., and Viers, B., J. of Fluid Engineering, Vol.114, pp113-118, (1992).
6. Lefebvre, A. H.," Atomization and Sprays", Hemisphere Pub. Corp., New york, (1989).

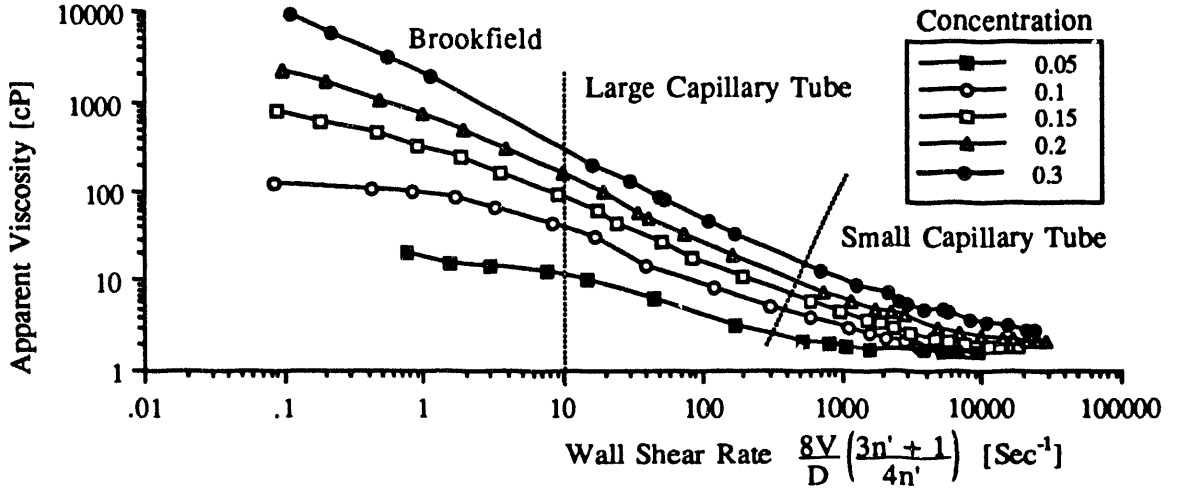

Fig. 1 Shear Viscosity Data Xanthan Gum Solutions

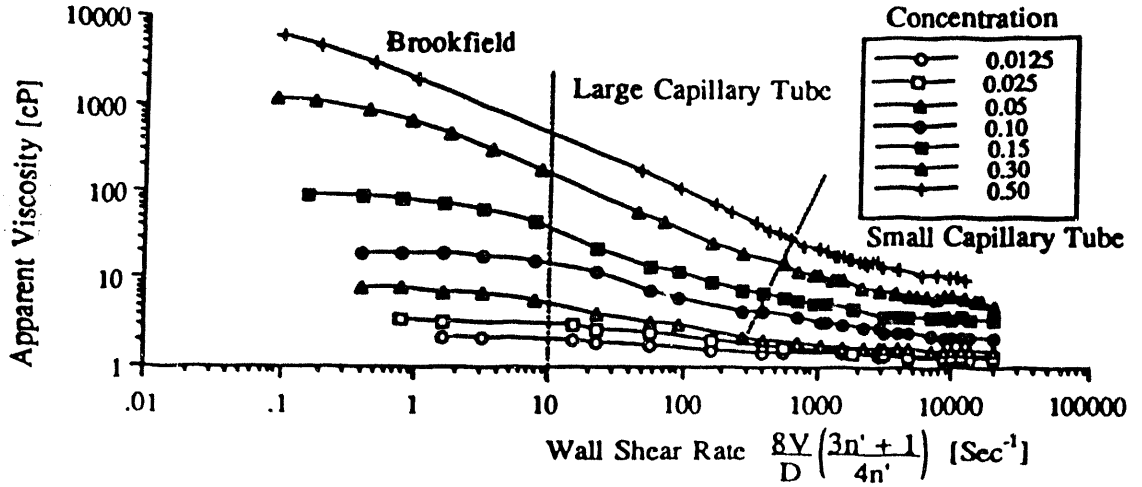

Fig. 2 Shear Viscosity Data Polyacrilamide E10 Solutions

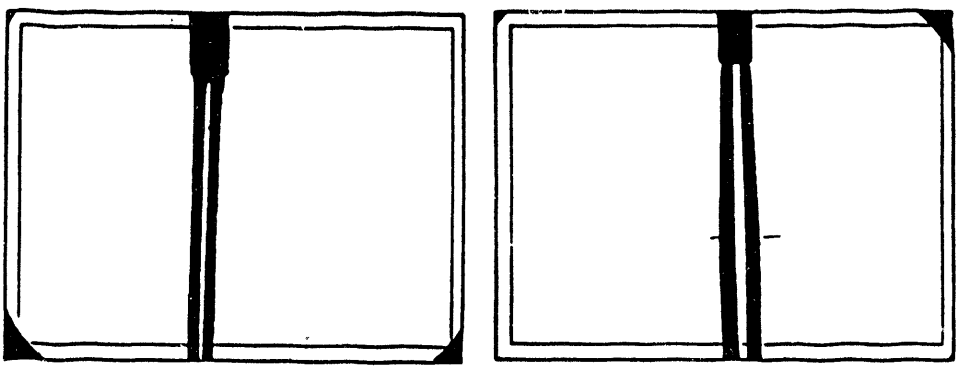

Fig.3 Die-Swell a) 0.3% Xanthan Gum, b) 0.5% E10 at 8V/D = 5246 S^{-1}.

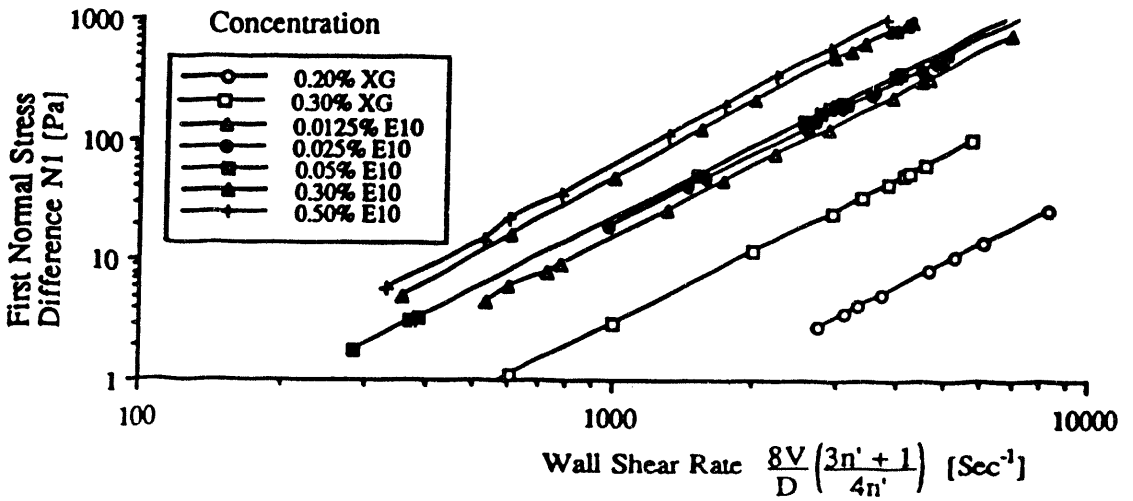

Fig. 4 First Normal Stress Difference

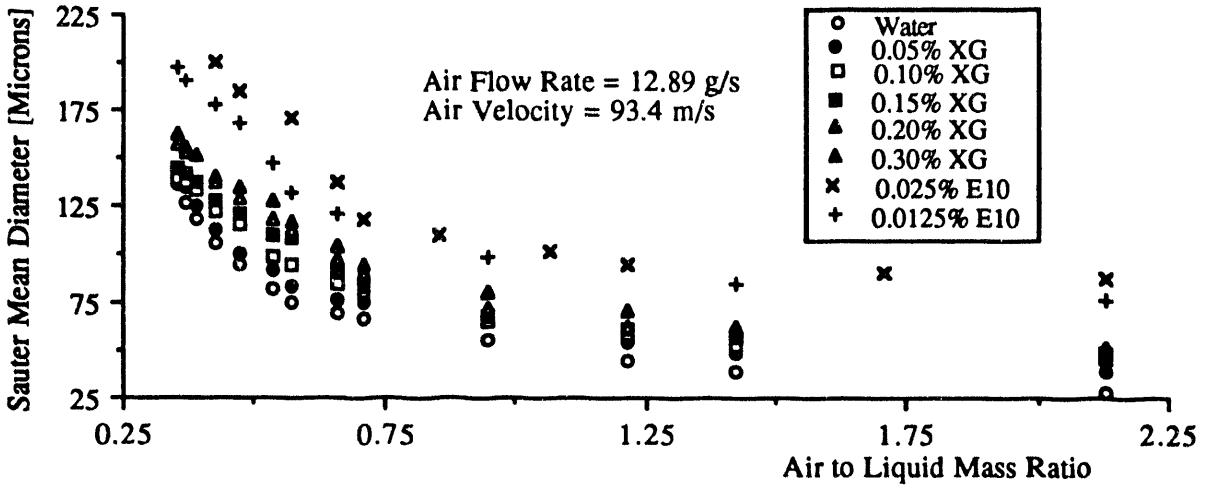

Fig.5 Variation of SMD as a function of Air/Liquid Ratio

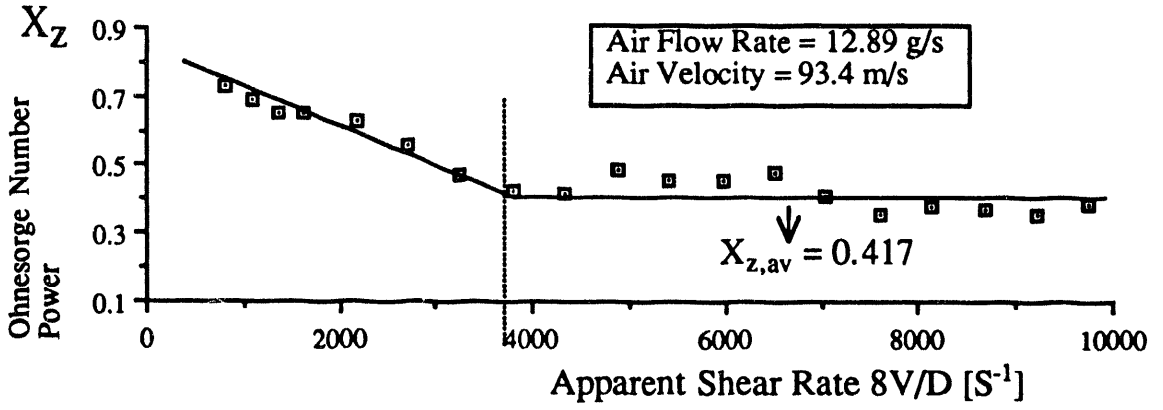

Fig. 6 Power Dependence of SMD on Ohnesorge (Z) Number at Various Shear Rates

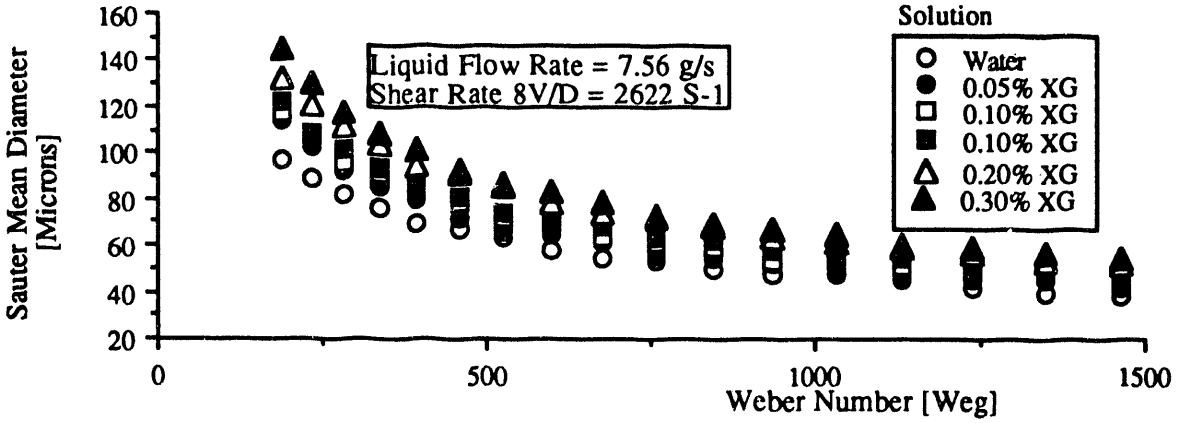

Fig. 7 Variations of SMD with Weber Number

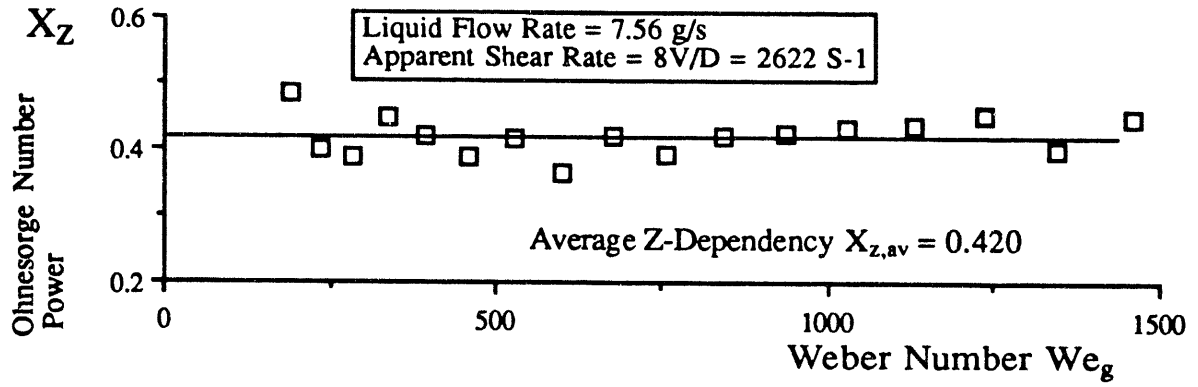

Fig. 8 Power Dependence of SMD on Ohnesorge (Z) Number at Various Weber Numbers

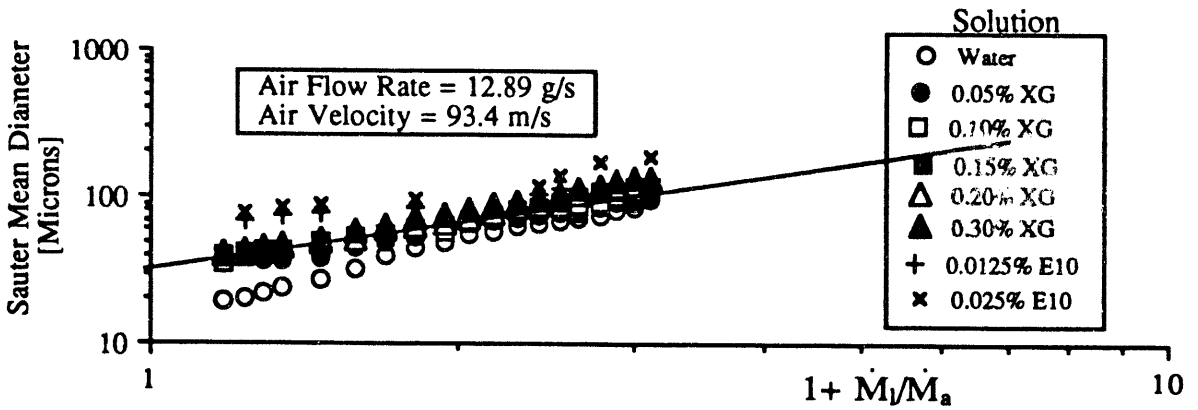

Fig. 9 Variation of SMD with $1+M_l/M_a$

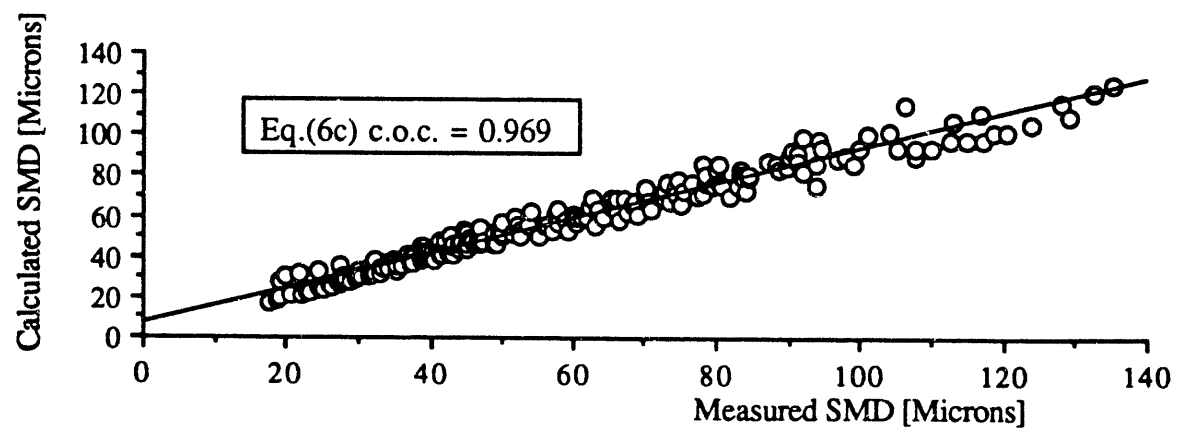

Fig.10 Calculated (by Eq. (6c)) vs Measured SMD

The following manuscript was unavailable at the time of publication.

THE ECONOMICS OF INDUSTRIAL BOILER RETROFITS TO FIRE COAL-BASED FUELS

A. Rose
Pennsylvania State University
222 Walker Bldg.
University Park, PA 16802

Please contact author(s) for a copy of this paper.

KRAKOW CLEAN FOSSIL FUELS AND ENERGY EFFICIENCY PROJECT

BARBARA L. PIERCE AND THOMAS A. BUTCHER
DEPARTMENT OF APPLIED SCIENCE
BROOKHAVEN NATIONAL LABORATORY
UPTON, NEW YORK 11973

Almost half of the energy used for heating in Krakow is supplied by low-efficiency boilerhouses and home coal stoves. Within the town, there are more than 1,300 boilerhouses with a total capacity of 1,071 MW, and about 100,000 home furnaces with a total capacity of about 300 MW. More than 600 boilerhouses and 60 percent of the home furnaces are situated near the city center. These facilities are referred to as "low emission sources" because they have low stacks. They are the primary sources of particulates and hydrocarbons in the city, and major contributors of sulfur dioxide and carbon monoxide.

The Support for Eastern European Democracy (SEED) Act of 1989 directed the U.S. Department of Energy (DOE) to undertake an equipment assessment project aimed at developing the capability within Poland to manufacture or modify industrial-scale combustion equipment to utilize fossil fuels cleanly. This project is being implemented in Krakow as the "Krakow Clean Fossil Fuels and Energy Efficiency Project." Funding is provided through the U.S. Agency for International Development (AID). The project is being conducted in a manner that can be generalized to all of Poland and to the rest of Eastern Europe.

PROJECT DESCRIPTION

The project details have been developed through extensive working contacts between DOE and Polish representatives. The project plan includes three phases which have been developed around five specific subprojects. The five specific subprojects include:

Subproject 1. Extensions to the district heating system to allow elimination of smaller, local boilerhouses which are more polluting than the central sources of heat. This subproject also includes building conservation activities which can allow elimination of additional local boilerhouses.

Subproject 2. Conversion of small, hand-fired boilers to natural gas or replacement with advanced coal combustion options.

Subproject 3. Elimination of home stoves by increased use of electric heating in selected parts of the city.

Subproject 4. Modernization of boilerhouses through replacement of existing boilers with modern units or refitting existing boilers to improve operations and reduce emissions.

Subproject 5. Use of improved home stove designs and/or improved coal fuels to reduce emissions.

In Phase I, testing and analytical activities are establishing the current level of emissions from existing equipment and operating practices, and will provide estimates of the costs and emission reductions of various options. Phase II consisted of public meetings in both Poland and the United States to present the results of Phase I activities. These meetings provided information to private firms who may be interested in forming joint ventures to implement recommendations from Phase I. In Phase III, DOE issued a solicitation for Polish/U.S. joint ventures to perform commercial feasibility studies for the use of U.S. technology in one or more of the areas under consideration. The solicitation closed in January, 1993, and awards were made last year.

This report provides results from Phase I. The Phase I studies involve efforts both on the Polish and the U.S. side. Because of the emphasis on conservation in Subproject 1, DOE's Office of Conservation and Renewable Energy is the lead DOE office for this subproject; subproject 1 results are not included in this report. Subprojects 2 through 5 are being managed by DOE's Office of Fossil Energy through the Pittsburgh Energy Technology Center (PETC). Brookhaven National Laboratory (BNL) as well as Burns and Roe Services Corporation (B&RSC) are supporting PETC. Work in Krakow is being managed by the Biuro Rozwoju Krakowa (BRK or Krakow Development Office) and for Subprojects 2 through 5 BRK is working under subcontract to BNL.

RESULTS TO DATE

Each subproject includes testing, engineering analysis, and incentive analysis components, as appropriate. Boiler and stove testing activities have been completed. These tests established baseline performance and emissions using current fuels and operating conditions, as well as alternative fuels and operating conditions. The engineering analyses include evaluation of local and regional air quality improvements due to the various alternatives considered, as well as cost estimates for conversions or replacements.

The incentive analyses include fuel price projections, economic analyses, examination of any legal or regulatory impediments to the various alternatives, and recommendations to the local government on ways to encourage implementation of those alternatives found to be worthwhile. In addition, a public relations effort has been defined to inform the citizens of Krakow about the project and provide the means for public attitudes to be measured and incorporated into project decision-making.

Testing

Boilers

About 77 percent of the boilers in Kraków, representing 86 percent of the capacity and almost 90 percent of the fuel use, are solid-fuel fired. More than 370,000 metric tons of coal and coke are consumed annually in the boilers. Testing was done at four sites - two with larger, mechanical stoker-fired boilers and two with hand-fired boilers. All boiler tests have been completed.

The hand-fired boilers tested include one site with cast iron boilers designed for coke firing, "Rydla Street," and one site with steel boilers, "Ułanów Street." Testing of the cast iron boilers at the Rydla boiler house was done with coke, with a coal/coke mixture and with smokeless briquettes produced by the Institute for the Chemical Processing of Coal, Zabrze, Poland. In addition to different fuels some different operating procedures were also evaluated. These included the introduction of overfire air and stoking the fuel in thinner layers at the grate. This last procedure obviously requires more frequent stoking.

Tests at Ułanów Street were performed with coal, a 70% coke/30% coal blend, and briquettes. The test program included effects of fuel type, load, and fuel bed layering. Effects of overfire air which were evaluated at the Rydla Street site were not evaluated at Ułanów.

As expected, results showed the highest particulate emissions with coal; wherever possible these units should change to coke or coal/coke mixtures. For steel boilers which cannot burn coke, briquettes should be considered. The hand-fired boilers are the dominant sources of CO and the organics. Changing from coal toward coke use in these boilers will reduce emissions of the organics but not CO. Based on experience gained during the testing program, it may be useful to explore the use of forced, distributed secondary air injection over the fire bed to reduce CO production in these boilers. In all cases overfire air should be used at the beginning of the firing cycle to minimize CO and volatile organics emissions.

Both of the stoker-fired boilers that were tested are owned and operated by MPEC, Kraków's heat distribution utility. The Krzesławice boiler house contains four identical PLM-2.51 boilers with total thermal capacity of

11.63 MW. One of these was tested during this program. The boilers are used to produce steam for nearby industries and operate all year. These boilers cannot, practically, be connected to the district heating system and are considered to be excellent candidates for modernization or replacement. Each boiler is equipped with a bank of six cyclones and an induced draft fan. During tests at this site, measurements were made before and after the cyclones to allow cyclone particulate removal efficiency to be determined.

Properties of all fuels tested at Krzeslawice are listed in Table 1. The normal, baseline fuel is Ziemowit. It is generally agreed that the Ziemowit coal contains more fines than is considered correct for boilers of this type, and one objective during the test was to evaluate benefits of a graded coal. Staszic III coal is a sample of the run-of-mine coal from the Staszic mine in Silesia (Staszic I) which has been washed and graded. Measurements of as-fired size distributions during the test program, however, indicated that Staszic III still contained more fines than is considered optimal. It is suspected that the coal was graded well at the mine but broke during shipping and handling. The final coal listed as "pea coal" was considerably coarser.

In baseline tests with Ziemowit coal excess air could not be reduced below about 150% at high load without leading to clearly excessive unburned carbon losses. As load is reduced, even higher excess air levels (200 - 300%) are required. Most of this excess air is simply uncontrolled casing leaks - even though an effort was made to seal the casing prior to the start of the test program. In addition, flue gas exit temperature was higher than specified in the design. Together, the high excess air and high gas temperature lead to very low efficiency for this boiler - from 56 to 72%. Boilers of this type should be capable of operating with excess air levels less than 100 percent and with thermal efficiencies from 77 to 87%. Under optimal operating conditions, the ash carbon content was about 10% - leading to thermal efficiency loss due to unburned carbon of about 4%. The cyclone dust collector efficiency ranged from 70 to 95% during the test program.

Relative to the fuel normally used at this site -Ziemowit - the Staszic coals and especially the washed Staszic III coal, gave reduced emissions and marked improvements in efficiency. In contrast, performance with the "pea coal" was very disappointing. During operation, this coal burned vigorously very close to the point at which it first fell on the grate. This led to poor distribution of heat release on the bed and high flue gas exit temperatures.

The Balicka boiler house provides hot water to a local part of the district heating system. The boiler tested was built in 1972 and is one of seven at Balicka. Test fuels at Balicka included the normal fuel, Ziemowit, and again unwashed and washed coals from the Staszic mine. Normal practice at this site calls for all air dampers to remain fixed for the entire operating season, a practice which leads to very high excess air (to 500%) at low loads and low thermal efficiency (52%). Attempts to vary overall excess air were not successful. Emission factors were generally similar to the baseline conditions at Krzeslawice. No significant improvements were realized with the use of alternative fuels, such as the washed Staszic coal or with the use of the overfire air. This somewhat surprising result may be largely due to the limited ability to control air flows at this site.

All of the results of this testing program lead to some conclusions about approaches which could, at least from a technical perspective, have the most immediate impact on emission of pollutants from Kraków's boilers. In the case of the hand-fired boilers, clearly coke use should be promoted. Also, all stokers should have particulate controls. The efficiency of the stoker-fired boilers is low. Improvements in instrumentation, controls, and mechanical conditions would allow operators to gain about 15% in efficiency with corresponding

Table 1. Test Fuels: Stoker-Fired Boiler at Krzeslawice

Fuel properties as-fired		Ziemowit Coal	Staszic I Coal	Staszic III Coal	Pea Coal
Water	%	17.4	17.4	7.6	12.4
Ash	%	22.9	23.1	6.1	4.6
Volatiles	%	27.2	26.9	30.9	33.7
Sulfur	%	1.5	0.73	0.72	0.52
Lower Heating Value	kJ/kg	19014	21918	26840	25212

reductions in pollution. The use of improved fuels at the stoker would be beneficial but only if the fuel switch is combined with an effort to optimize performance. An effort of this type must include adequate instrumentation to accurately determine performance changes.

Stoves

There are approximately 100,000 coal-fired tile stoves in Kraków with an annual coal consumption of 130,000 metric tons. It has been estimated that there are about 7 million of these stoves throughout the country of Poland. The masonry tile stove tested during this program is typical of those used in Kraków. It was built specifically for these tests by local craftsmen in a laboratory at the Academy of Mining and Metallurgy. The testing system uses a dilution tunnel method to determine gaseous pollutant emission rates and flue gas energy loss on a continuous basis. Particulate emissions are averaged over firing cycles.

Properties of the fuels evaluated during this testing program are listed in Table 2. The two coals listed represent the best and worst fuels currently used in Kraków. Coal from the Boleslaw Smialy mine is high in ash content and low in heating value and currently sells for about $60/metric ton. Wujek coal is much better in quality and higher in price--about $80/ton. The "Zabrze" briquettes have been produced by the Institute for the Chemical Processing of Coal in Zabrze, Poland in a pilot-scale facility. These briquettes are termed "smokeless" because of their reduced volatiles content. The wood briquettes have been made from wood waste and are currently about half the price of coal (per-ton basis). The final fuel listed is a coke which has also been recently offered as a possible option for the home stoves.

Performance of the tile stove is summarized in Table 3. Generally, the efficiency of the tile stove was found to be higher than expected. A dramatic reduction in particulate emissions is obtained by substituting the smokeless briquettes for the coal. Carbon monoxide emissions, however, were found to increase sharply with this fuel and this result is unacceptable. With the smokeless briquettes combustion was very slow--leading to the low values of NO_x emissions with this fuel. Also the stove mass temperature rise during firing was considerably lower with the briquettes. This is consistent with the lower stove efficiency listed in Table 3.

In the baseline tests the results with the smokeless briquettes were very encouraging for the possibility of reducing particulate emissions. To reduce CO emissions, several methods of increasing the burning zone temperature were then evaluated including: 1) the use of two types of metal inserts designed to increase air flow through and reduce heat loss from the fuel bed and, 2) packaging the briquettes in combustible containers. These efforts were essentially not successful.

During the course of the investigations, however, an improved operating procedure was developed which was successful in improving performance. This new procedure involves feeding the fuel onto the grate in 3 equal parts, one during the ignition and the other two during the process of combustion; reducing the overall excess air and, at the same time, supplying all of the combustion air through the lower, ash pit, door (obviously except when adding fuel or grooming the bed); more frequent poking of the bed; and closing the bottom door,

Table 2. Coal Stove Test Fuels

Fuel properties as-fired		Boleslaw Smialy Coal	Wujek Coal	Zabrze Briquettes	Wood Briquettes	Coke
Water	%	2.5	2.72	3.3	5.6	0.1
Ash	%	21.6	3.32	10.9	1.8	8.7
Volatiles	%	30.3	32.1	8.1	71.6	1.0
Combustible Sulfur	%	.3	0.3	0.2	0.0	0.5
Lower Heating Value	kJ/kg	24505	31324	27619	17916	30280

Table 3. Stove Test Results

		Boleslaw Smialy Coal	Wujek Coal	Zabrze Briquettes	Wood Briquettes	Coke
Efficiency	%	62	68 [75.1]	57 [73.6]	74	[73.1]
Particulates	g/kg	13.8	16.6 [15]	0.8 [1.2]	6.4	[1.8]
CO	g/kg	20	27.1 [32]	49.3 [21]	48.4	[28]
Semivolatile Organics	g/kg	0.9	0.9 [1.9]	0.4 [0.54]	2.05	[0.55]
Volatile Organics	g/kg	3.4	1.8 [3.9]	2.4 [1.4]	6.0	[1.8]
NOx	g/kg	3.3	6.9 [2.8]	2.4 [1.8]	0.5	[1.6]
SO2	g/kg	5.6	5.1 [2.7]	3.3 [4.1]	0.07	[2.8]
Note: Modified Operating Procedure results are given in brackets.						

effectively ending combustion, earlier. Specifically, the bottom door was closed just after the flue gas leaving the stove reached peak temperature. The last part of the procedure is an important one because CO emissions always increase dramatically at the end of the normal operating procedure. Closing the door earlier may lead to higher amounts of unburned coke remaining on the grate. However, this coke is burned during the next firing cycle and does not lead to an efficiency loss. It should be noted that as part of the test procedures used during this program efficiency was evaluated during multiple cycles, not just a single firing.

Testing with the improved operating procedure was done with three selected fuels - Wujek coal, the smokeless briquettes, and coke. Results are listed in brackets in Table 3. Relative to the baseline tests the new procedure gave dramatic improvements in thermal efficiency and reductions in CO with the low volatile content briquettes. Using this procedure with smokeless fuels leads to clear reductions in emissions.

Table 4 compares total emissions from the different low-stack sources. Among the categories listed, the home stoves do not consume the most coal. They are, however, by far the most important single source of particulates and semivolatile organics. They are, in addition, important sources of both volatile organics and CO. Changing the fuel to briquettes or coke and using the improved operating procedures developed here would reduce stove particulate, CO, and semivolatile organics emissions. This would clearly have a great impact on Kraków's air quality. This change would require no capital investment by Kraków residents.

Engineering Analyses

For each subproject an engineering analysis has been or will be undertaken. The purpose of the engineering analysis is to determine: 1) the part of the City which is appropriate for the subproject; 2) the technical scope required; and 3) the captial costs of conversion. Most of the engineering analyses have been completed.

Gas Conversion

Converting solid-fuel fired boilers to gas is the option of choice for the Old Town area of Kraków. This is primarily because the oldest part of the City is inaccessible to the district heating network. More than 20 years ago the City began a program of conversion, but there are still at least 36 solid-fuel fired boiler houses (capacity 16 MW) remaining to be converted. All but one could be converted to gas, with only minor modifications to the distribution system. Total costs would be about $2 million, or $125/KW. An additional engineering analysis was completed for an area adjacent to Old Town. There are 195 boiler houses operating there, of around 95 MW combined output. Extension of the low- and medium-pressure distribution systems

Table 4. Comparison of Contribution of Boilers and Home Stove to Kraków Emissions

		Annual Emissons (metric tons per year)					
	Fuel Use (MT/yr.)	Particulates	CO	Semivolatile Organics	Volatile Organics	NOx	SO2
Stoker without cyclones	34984	539	290	1	0	77	1025
Stokers with cyclones	198240	427	1645	6	0	436	5808
Hand-Fired Boilers-coke	59107	118	5467	4	41	112	1046
Hand-Fired Boilers - coal/coke mixtures	52023	281	3871	57	328	62	931
Hand-Fired Boilers - coal	26012	520	1171	42	75	60	471
Home Stoves - coal fired	130000	2158	3523	117	221	455	663

would cost about $2 million, and boiler conversion would cost $10.5 million. An analysis of the high pressure part of the supply system is currently underway. If all boiler houses in the areas adjacent to the Old Town that cannot be reached by the municipal district heating network are converted to gas, with a reserve towards gas heating for buildings now using home stoves, a significant increase in gas supply will be be required.

Electric Conversion

Both in the past and at present, a significant number of residents would be willing to cover the cost of changing from heating by coal-fired stoves to electric space-heating. The obstacle to more widespread adoption of this conversion is the lack of transformer stations and cable networks distributing power from the main power supply points (MPSPs) and supplying each building with heating stoves. One area of the City, immediately adjacent to the Old Town, has been deemed appropriate for conversion of home stoves to electric heat. This area includes many buildings heated by stoves, and the newly-erected ŁOBZÓW MPSP with a reserve capacity of about 50 MW that can be used for heating.

The engineering analysis has determined that around 8,500 coal stoves in this area can be converted to electric heating with the construction of 78 transformer stations, 15/0.4 kV; 19.4 kilometers of medium-voltage cable network; and 19.0 kilometers of low-voltage cable network. The total cost of these capital projects is around $2.4 million. In addition, the cost of converting each stove is about $200. The total installed capacity will be 18.1 MW, and the total average cost is $227/KW. The analysis was extended to include the remaining 3,100 stoves in the Old Town, because the demand for power in the Łobzów area will not use all the reserve capacity of this station. The power output installed in these stoves would be 8.7 MW; average cost of conversion in the Old Town will be USD 138 per KW.

Modernization of Boilerhouses

Not all the solid fuel boiler houses in Kraków could be eliminated by connecting them to the district heating network, nor improved in terms of emissions by conversion to natural gas. The town has more than 100 solid fuel boilerhouses of a combined output of around 250 MW, operated throughout the year, producing either process steam or domestic hot water. These boiler houses should continue on solid fuels, with necessary upgrades to lessen the impact of the combustion process on the environment.

One of the boilers at the Krzesławice boiler house was selected for evaluation of modernization options. The engineering analysis was carried out by two teams - American and Polish. The American team adopted American technology and equipment; the domestic team used Polish technology and equipment. Design options included stoker boilers with traveling grates and fluidized bed boilers with different operating characteristics and emissions control approaches. Oil-fired boilers were also evaluated. Although the capital cost of oil boilers is the cheapest among the options, they are not competitive overall due to the very high price of oil in Poland.

Options involving imported equipment have high capital costs, due to the high exchange rate between the Polish zloty and the U.S. dollar, and the severalfold difference in labor costs. In all modernization options involving coal-fired boilers there is a drop in fuel consumption due to improved efficiency. This allows savings in fuel cost as well as in labor and environmental fees. Capital costs range from $220/MW to $900/MW, and operating costs from $62/MW to $81/MW.

Air Quality Analysis

Air quality analyses in the Kraków project are being carried out following the completion of engineering analyses. Air quality modeling follows Pasquille's formula in the version adopted in Poland according to the guidelines of the Ministry of Environmental Protection. The amount of emissions (concentrations of pollutants) are related to annual standard values, i.e. 32 μ/m^3 for SO_2 and 50 μ/m^3 for particulates. In the city center these values are exceeded threefold and more.

Recent work has focused on home stove options - converting to gas or electricity, or switching to briquettes. Results show that switching to briquettes achieves almost the same benefits as converting the stoves. The concentrations of particulates and SO_2 drop within the city center by an amount equal to the standard permissible load. These results confirm the efficacy of using "clean" coal, even if only in a transitional period.

Incentives Analysis

The primary objective of incentives analysis is to define and evaluate incentives that the City could offer to encourage implementation of options under investigation in this project. Based on an economic analysis of each of these options, possible incentives are identified. The incentives are then evaluated in terms of their technical and legal feasibility, cost, and effectiveness. Incentives analysis for one of the subprojects, converting Old Town boilers to natural gas, has been completed.

The economic analysis showed that conversion to gas is not economic for boiler owners. The analysis further showed that providing a subsidy for conversion costs would be less expensive for the City than subsidizing the price of heat. The legal analysis showed that although the City cannot impose new taxes (this can only be done by referendum), there are several ways the City could provide incentives to encourage conversion. The City has the authority to set property tax rates, and may also create property tax exemptions as a subsidy to boiler house owners. The City controls rents for some of the buildings, and may lower or freeze rents to encourage conversions. The City also has the authority to order conversions. Finally, the City could create an environmental fund with its share of the revenues from fines and fees for use of the environment and use these funds to support conversions.

Public Relations

A public opinion survey was administered to the residents of Kraków. Results show that most residents consider air pollution to be an important issue and that most residents consider industry and traffic to be the main sources of air pollution. A significantly higher portion of Old Town residents feel that the low-stack sources are the most important sources, however. While residents state that they are willing to pay to reduce pollution, the amount that they are willing or able to pay is probably not sufficient. Residents also feel that City authorities should take responsibility for cleaning the air.

Based on the survey results, a public relations campaign has been defined to inform Kraków's residents about the low-stack sources and about this project. This is being done through press releases and briefings for journalists, seminars, and production of brochures and educational films.

FUTURE PLANS

In Phase I, the primary tasks remaining are to complete the incentives analyses for the home stove options. Planning is underway, and the analyses should be finished this year. In addition, BNL and BRK will prepare a joint report summarizing all the Phase I activities.

Further, Phase I activities are being extended to provide wider communication of the results of Phase 1, both within Kraków and to other cities. These activities include a workshop in Kraków directed to potential funding institutions, Kraków utilities, and city and provincial government representatives. BRK will update the survey of the City's boiler population, and link the survey to a geographical information system. BRK will also work with the City by providing details for city planning, including the impacts of the Phase III projects. Finally, BRK will meet with representatives of other cities to share the information, tools and experiences of the Kraków Program. A conference for this purpose was held in Plzen in April 1994.

The solicitation for Phase III was issued in September 1992. Final awards to eight firms were announced in September 1993. Two projects address the district heating system, five address the reductio of emissions from boilers, and one addresses the home stoves. Cooperative Agreements are being finalized this spring, and the projects will be completed in two to four years.

REFERENCES

EKOPOL. "Estimation of Air Quality Improvement at the Town, Which Could be Reached After Switch Over from Stove Heating to Electric or Gas Heating Combined with the Application of Improved Furel Sorts," December 1993.

Energoekspert. "Testing of PLM-2.5-1 Boiler No. 3 in the Krzeslawice Boiler House," 1992.

Energoekspert. "Testing of Type ECA-IV Boilers in the ul. Rydla 28 Boiler House," 1993.

Energoekspert. "Testing of Steel Heating Boilers in the ul. Ulanow Boiler House," 1993.

Gyorke, Douglas F. "Pittsburgh Energy Technology Center's Overview of the Kraków Projects," presented at *Converence on Alternatives for Pollution Control from Coal-Fired Low Emission Sources*,' Plzen, Czech Republic, April 1994.

Krakow Development Office. "A Conceptual Study of GPZ "Lobzow" Electric Energy Distribution System for Replacing Stove Heating with Electric Heating, Together with Cost Estimate," Volumes I and II, July 1992.

Krakow Development Office. "Analysis of Feasibilities of Coal to Natural Gas Boiler House and Stove Heatings Conversion Within the Area of II Ring Road," May 1993.

University of Mining and Metallurgy. "Research on Possibilities of Reduction of Noxious Emissions Through Combustion Modification," December 1993.

VRG Strategy Co. Ltd. "Assessment of Attitudes Toward Low Emission Pollution Amongst Residents of Cracow," April 1993.